Path Optimization by a Variational Reaction Coordinate Method I. Development of Formalism and Algorithms

Adam B. Birkholz and H. Bernhard Schlegel[1]

Department of Chemistry, Wayne State University, Detroit,
Michigan 48202

The development of algorithms to optimize reaction pathways between reactants and products is an active area of study. Existing algorithms typically describe the path as a discrete series of images (chain of states) which are moved downhill toward the path, using various reparameterization schemes, constraints, or fictitious forces to maintain a uniform description of the reaction path. The Variational Reaction Coordinate (VRC) method is a novel approach that finds the reaction path by minimizing the variational reaction energy (VRE) of Quapp and Bofill. The VRE is the line integral of the gradient norm along a path between reactants and products and minimization of VRE has been shown to yield the steepest descent reaction path. In the VRC method, we represent the reaction path by a linear expansion in a set of continuous basis functions and find the optimized path by minimizing the VRE with respect to the linear expansion coefficients. Improved convergence is obtained by applying constraints to the spacing of the basis functions and coupling the minimization of the VRE to the minimization of one or more points along the path that correspond to intermediates and transition states. The VRC method is demonstrated by optimizing the reaction path for the Mller-Brown surface and by finding a reaction path passing through 5 transition states and 4 intermediates for a 10 atom Lennard-Jones cluster.

04 June 2025 14:14:31

I. INTRODUCTION

The steepest descent reaction path (SDRP) can be readily determined by walking downhill from a transition state on the potential energy surface. When defined in mass-weighted cartesian coordinates, this pathway is also known as the intrinsic reaction coordinate[1]. The SDRP provides a first-order approximation of the route that a chemical system follows as a reaction proceeds from reactants to products. While various methods are able to readily follow the reaction path once the transition state is known (see reference[2] for a recent review of methods), locating the transition state can often be a difficult task. One common approach that is used to approximate the minimum energy path without a converged transition state structure is to express the pathway as multiple discrete geometries, or images, which are optimized simultaneously (for leading references, see[3–14]). These chain of states methods typically begin with a series of images along an interpolation between reactants and products, after overall translation and rotation have been removed. The images are updated to minimize the energies of each point subject to constraints, fictitious forces or interpolation/reparameteration schemes, which ensure that the points maintain a uniform description of the pathway. In these methods, the optimizer is generally required to take small steps in order to avoid the introduction of kinks in the path. This ad-hoc approach also has the drawback that it is not variational, so there is no reliable way of determining whether or not the optimization is making good progress, or if a solution found is in fact a minimum.

04 June 2025 14:14:31

Recently, the line integral of the gradient norm has been described as a variational property of a reaction path. The line integral of the gradient norm is expressed as

$$\begin{aligned} E_{VRE} &= \int_{t_R}^{t_P} \sqrt{\frac{\partial V\left(\mathbf{x}\left(t\right)\right)}{\partial x}^{\mathrm{T}} \frac{\partial V\left(\mathbf{x}\left(t\right)\right)}{\partial x}} \sqrt{\frac{d\mathbf{x}\left(t\right)}{dt}^{\mathrm{T}} \frac{d\mathbf{x}\left(t\right)}{dt}} dt \\ &= \int_{t_R}^{t_P} \left|\mathbf{g}\left(\mathbf{x}\left(t\right)\right)\right| \left|\boldsymbol{\tau}\left(t\right)\right| dt \end{aligned} \tag{1}$$

where V is the potential energy, $\mathbf{x}\left(t\right)$ are the coordinates of the reaction path parameterized by t, t_R and t_P are the parameter values corresponding to the reactant and product structures, respectively, while $\mathbf{g}$ and $\boldsymbol{\tau}$ are used as shorthand for the gradient of the potential energy surface, and the tangent to the path. This integral is a non-negative, energetic quantity, and will be referred to as the Variational Reaction Energy (VRE) throughout this work. Rigorous proofs that the VRE is minimized by the steepest descent reac-

tion path are discussed work by Quapp, Bofill and others[15–17]. A simple conceptual proof can be obtained by computing the VRE while assuming that $\mathbf{x}(t)$ is the steepest descent path. On the SDRP, the gradient is everywhere proportional to the tangent, therefore $|\mathbf{g}(\mathbf{x}(t))|\,|\boldsymbol{\tau}(t)| \equiv \left|\mathbf{g}(\mathbf{x}(t))^T \boldsymbol{\tau}(t)\right|$. This simplifies the VRE to the absolute value of the projection of the gradient onto the tangent, which may be evaluated exactly as the sum of the energy differences between maxima and their adjacent minima along the path *(E_{pVRE})*

$$\begin{aligned} E_{pVRE} &= \int_{t_R}^{t_P} \left|\mathbf{g}(\mathbf{x}(t))^{\mathrm{T}} \boldsymbol{\tau}(t)\right| dt \\ &= \sum_a \left(2V(\mathbf{x}_{a,TS}) - V(\mathbf{x}_{a,P}) - V(\mathbf{x}_{a,R})\right) \end{aligned} \tag{2}$$

where a in the sum is over the number of barriers along the path, and $\mathbf{x}_{a,R}$ and $\mathbf{x}_{a,P}$ are the local minimum structures adjacent to the corresponding local maximum $\mathbf{x}_{a,TS}$. Away from the reaction path, this projected VRE may still be evaluated according to the sum in eqn 2, but the reaction path will no longer be proportional to the tangent and $|\mathbf{g}(\mathbf{x}(t))|\,|\boldsymbol{\tau}(t)| > \left|\mathbf{g}(\mathbf{x}(t))^T \boldsymbol{\tau}(t)\right|$. Consequently, the VRE is always greater than or equal to the projected VRE for any path connecting the same reactant and product structure, and updating a path to minimize the VRE will lead to the SDRP. This also provides a useful non-negative estimate for the variational error in the current path

$$\begin{aligned} \epsilon &= E_{VRE} - E_{pVRE} \\ &= \int_{t_R}^{t_P} |\mathbf{g}(\mathbf{x}(t))|\,|\boldsymbol{\tau}(t)|\,dt - \sum_a \left(2V(\mathbf{x}_{a,TS}) - V(\mathbf{x}_{a,P}) - V(\mathbf{x}_{a,R})\right) \end{aligned} \tag{3}$$

Methods to minimize E_{VRE} by a chain of states approach have been discussed elsewhere[15], but these suffer from many of the same problems that exist in the ad hoc path optimization methods. Many small steps are required to converge the path and the discretization error can result in non-variational behavior unless many images are used. Since E_{VRE} is a functional of a smooth, continuous object, it should be advantageous to describe the path using a continuous representation such as a basis set expansion. Such a representation provides a set of coordinates, the linear expansion coefficients (LEC), which can be optimized by minimization of E_{VRE} using standard gradient-based optimization methods. The following work describes the development of a proof of concept for the Variational Reaction Coordinate (VRC) method, and demonstrates the effectiveness of the method on a number of test problems.

04 June 2025 14:14:31

II. PATH OPTIMIZATION BY VRC

A. A continuous description of the reaction path

In the VRC method, a continuous representation is used to model the reaction path. This has the benefit of eliminating the need to select discrete points for optimization, as well as the amiguities involved with defining the tangent as a function of those points. To facilitate the optimization of the path, the continuous representation should depend on a set of parameters that may be varied. A basis set expansion expresses the path in terms of a set of n_{basis} continuous functions and linear expansion coefficients (LEC, $C_{i\mu}$)

$$\begin{aligned} x_i(t) &= \sum_{\mu=1}^{n_{basis}} C_{i\mu}\phi_\mu(t) \rightarrow \frac{\partial x_i(t)}{\partial C_{i\mu}} = \phi_\mu(t) \\ \tau_i(t) &= \sum_{\mu=1}^{n_{basis}} C_{i\mu}\frac{d\phi_\mu(t)}{dt} \rightarrow \frac{\partial \tau_i(t)}{\partial C_{i\mu}} = \frac{d\phi_\mu(t)}{dt} \end{aligned} \tag{4}$$

where the Roman indices are over the $3 \times n_{atoms}$ cartesian coordinates that define the geometry, and the Greek indices are over the basis functions. The choice of t_R and t_P are completely arbitrary so long as non-zero portions of the basis functions span the space between them, so values of for $t_R = 0$ and $t_P = 1$ will be used throughout this work and functions will be chosen with the appropriate support. Polynomial spline functions are commonly used to represent the reaction pathway in discrete path optimization methods in order to produce smooth tangents, or to compute distances between points for constraints or reparameterizations. Therefore, we choose B-Splines[18] as the basis set expansion in the present work. B-Splines are a formulation of piecewise continuous polynomial splines, constructed in such a way that they may be expressed as a linear basis set expansion. The B-Spline basis are polynomials, and the number, range, shape and distribution of functions in the basis depends on the choice of the knot vector, $\mathbf{u}$. For the present work, a quartic basis with $n = n_{basis}$ LEC per coordinate is defined by n internal functions that span the range $0 < t < 1$, along with two capping functions which peak sharply at $t = 0$ and $t = 1$. The capping functions allow the geometries of the reactants and products to remain fixed by setting the corresponding LEC to the reactant and product geometries.

04 June 2025 14:14:31

The knot vector used in the present work is defined as follows

$$u_\mu = \begin{cases} 0 & 1 \leq \mu \leq d+1 \\ \sum_{\nu=\mu-d-2}^{\mu-1} \frac{\nu}{(n+1)(d+2)} & d+2 \leq \mu \leq n+2 \\ 1+10^{-10} & n+3 \leq \mu \leq n+d+3 \end{cases} \tag{5}$$

where $d = 4$ is the order of the polynomial, n is the number of internal basis functions, and the addition of 10^{-10} to the final knots ensures that $\phi(1)$ is defined without significantly impacting the shape of the final basis function. The final basis functions $\phi_{\mu=1}^{k=d}$ through $\phi_{\mu=n_{basis}}^{k=d}$ are given by the following recursion relation

$$\phi_\mu^0(t) = \begin{cases} 1 & u_\mu \leq t < u_{\mu+1} \\ 0 & \text{otherwise} \end{cases} \tag{6}$$

$$\phi_\mu^k(t) = \frac{t-u_\mu}{u_{\mu+k}-u_\mu}\phi_\mu^{k-1}(t) + \frac{u_{\mu+k+1}-t}{u_{\mu+k+1}-u_{\mu+1}}\phi_{\mu+1}^{k-1}(t) \tag{7}$$

with the derivative expressions and more efficient means of evaluating B-splines given in the reference[18]. Figure 1 demonstrates the shape of the basis functions when n is 5.

Once a choice of basis has been made, the VRE may be evaluated by an appropriate quadrature method. The determination of what is the most appropriate or efficient method is saved for a later investigation, and a simple adaptive quadrature method based upon a combination of 3rd order Gauss-Legendre and 5th order Curtis Clenshaw rules[19] will be used for the examples provided in this paper. The adaptive integrator evaluates the integral on a coarse grid as an extrapolation of the two quadrature rules, and computes an error based upon the difference between the two rules. Each interval on the integration grid is evaluated, and any intervals which have an error above a tolerance are evaluated again on a progressively finer grid. This process is repeated until the error for all intervals is below an absolute or relative tolerance. Once the VRE and it's derivatives have been computed, the energies of all of the PES evaluations used in the adaptive quadrature process can be compared in order to find local maxima/minima along the path for the purpose of computing ϵ_{VRE} and other terms that depend on the location of these stationary points.

04 June 2025 14:14:31

B. VRE derivatives

Having selected a set of coordinates to represent the path, the next step is to construct a local quadratic approximation (LQA, Q_{VRE}) to the VRE

$$\begin{aligned} Q_{VRE}(\mathbf{C}) &= E_{VRE}(\mathbf{C}_0) + \frac{\partial E_{VRE}(\mathbf{C}_0)}{\partial \mathbf{C}}^T \Delta\mathbf{C} + \frac{1}{2}\Delta\mathbf{C}^{\mathrm{T}} \frac{\partial^2 E_{VRE}(\mathbf{C}_0)}{\partial \mathbf{C}^2} \Delta\mathbf{C} \\ &= E_0 + \boldsymbol{\gamma}_0^T \Delta\mathbf{C} + \frac{1}{2}\Delta\mathbf{C}^{\mathrm{T}} \boldsymbol{\eta}_0 \Delta\mathbf{C} \\ \text{where } \boldsymbol{\Delta}\mathbf{C} &= \mathbf{C} - \mathbf{C}_0 \end{aligned} \tag{8}$$

where γ and η are used to represent the gradient and Hessian of the VRE with respect to a change in the LEC in order to avoid confusion with the gradient and Hessian of the potential with respect to a change in the molecular geometry, represented by $\mathbf{g}$ and $\mathbf{H}$, respectively. The formula for the VRE gradient is given below, with the explicit dependence on $\mathbf{x}$ and t dropped for brevity

$$\begin{aligned} \gamma_{i\mu} = \frac{\partial E_{VRE}}{\partial C_{i\mu}} &= |\mathbf{g}_P|\,|\boldsymbol{\tau}_P| \frac{\partial \mathbf{x}_P}{\partial C_{i\mu}} - |\mathbf{g}_R|\,|\boldsymbol{\tau}_R| \frac{\partial \mathbf{x}_R}{\partial C_{i\mu}} + \int_{t_R}^{t_P} \frac{\partial\left(|\mathbf{g}|\,|\boldsymbol{\tau}|\right)}{\partial C_{i\mu}} dt \\ &= \int_{t_R}^{t_P} \left(\frac{\partial |\mathbf{g}|}{\partial C_{i\mu}} |\boldsymbol{\tau}| + |\mathbf{g}| \frac{\partial |\boldsymbol{\tau}|}{\partial C_{i\mu}} \right) dt \end{aligned} \tag{9}$$

The two terms outside of the integral can be safely neglected since the coefficients corresponding to the capping functions are fixed, and the reactants and products do not vary with changes to the internal functions. Differentiating equation 9 a second time yields

$$\begin{aligned} \eta_{i\mu j\nu} = \frac{\partial^2 E_{VRE}}{\partial C_{i\mu} \partial C_{j\nu}} = \int_{t_R}^{t_P} \Bigg(& \frac{\partial^2 |\mathbf{g}|}{\partial C_{i\mu} \partial C_{j\nu}} |\boldsymbol{\tau}| + \frac{\partial |\mathbf{g}|}{\partial C_{i\mu}} \frac{\partial |\boldsymbol{\tau}|}{\partial C_{j\nu}} + \\ & \frac{\partial |\mathbf{g}|}{\partial C_{j\nu}} \frac{\partial |\boldsymbol{\tau}|}{\partial C_{i\mu}} + |\mathbf{g}| \frac{\partial^2 |\boldsymbol{\tau}|}{\partial C_{i\mu} \partial C_{j\nu}} \Bigg) dt \end{aligned} \tag{10}$$

The derivatives of the gradient norm and the tangent norm with respect to changes in LEC are straightforward to compute

$$\frac{\partial |\mathbf{g}|}{\partial C_{i\mu}} = \frac{\sum_a H_{ia} g_a}{|\mathbf{g}|} \phi_\mu \tag{11}$$

$$\frac{\partial |\boldsymbol{\tau}|}{\partial C_{i\mu}} = \frac{\tau_i}{|\boldsymbol{\tau}|} \frac{d\phi_\mu}{dt} \tag{12}$$

$$\frac{\partial^2 |\mathbf{g}|}{\partial C_{i\mu} \partial C_{j\nu}} = \left(\frac{\sum_a \left(\partial H_{ia} / \partial x_j\right) g_a + H_{ia} H_{ja}}{|\mathbf{g}|} - \frac{\sum_{a,b} H_{ia} g_a H_{jb} g_b}{|\mathbf{g}|^3} \right) \phi_\mu \phi_\nu \tag{13}$$

$$\frac{\partial^2 |\boldsymbol{\tau}|}{\partial C_{i\mu} \partial C_{j\nu}} = \left(\frac{\delta_{ij}}{|\boldsymbol{\tau}|} - \frac{\tau_i \tau_j}{|\boldsymbol{\tau}|^3} \right) \frac{d\phi_\mu}{dt} \frac{d\phi_\nu}{dt} \tag{14}$$

04 June 2025 14:14:31

Since the VRE depends on the potential energy gradient, the VRE gradient depends on the potential energy Hessian, and the VRE Hessian depends on the third derivative of the potential energy. However, in each of these cases, it is only the product of the higher derivative with the gradient that is necessary, which may be computed numerically by finite difference.

$$(Tg)_{ij} = \sum_a \frac{\partial H_{ij}}{\partial x_a} g_a \approx \frac{|\mathbf{g}|}{\delta} \left(H_{ij}(\mathbf{x}) - H_{ij}\left(\mathbf{x} - \delta \frac{\mathbf{g}}{|\mathbf{g}|} \right) \right) \tag{15}$$

Combining equations 9 and 10 with equations 11-15, the full expressions for the VRE gradient and Hessian are

$$\gamma_{i\mu} = \int_{t_R}^{t_P} \left(\frac{|\boldsymbol{\tau}|}{|\mathbf{g}|} \sum_a H_{ia} g_a \phi_\mu + \frac{|\mathbf{g}|}{|\boldsymbol{\tau}|} \tau_i \frac{d\phi_\mu}{dt} \right) dt \tag{16}$$

$$\begin{aligned} \eta_{i\mu j\nu} = \int_{t_R}^{t_P} \Bigg(& \frac{|\boldsymbol{\tau}|}{|\mathbf{g}|} \left((Tg + HH)_{ij} - \frac{\sum_{a,b} H_{ia} g_a H_{jb} g_b}{|\mathbf{g}|^2} \right) \phi_\mu \phi_\nu + \\ & \frac{\sum_a H_{ia} g_a \tau_i}{|\mathbf{g}|\,|\boldsymbol{\tau}|} \phi_\mu \frac{d\phi_\nu}{dt} + \frac{\tau_i \sum_a H_{ja} g_a}{|\mathbf{g}|\,|\boldsymbol{\tau}|} \frac{d\phi_\mu}{dt} \phi_\nu + \\ & |\mathbf{g}| \left(\frac{\delta_{ij}}{|\boldsymbol{\tau}|} - \frac{\tau_i \tau_j}{|\boldsymbol{\tau}|^3} \right) \frac{d\phi_\mu}{dt} \frac{d\phi_\nu}{dt} \Bigg) dt \end{aligned} \tag{17}$$

With the VRE gradient and Hessian computed, Newton's method can be used to find the LEC displacement corresponding to the minimum of a shifted VRE LQA (Eqn. 8)

$$\mathbf{\Delta C} = -\left(\boldsymbol{\eta} - \xi_\sigma \boldsymbol{\sigma} \right)^{-1} \boldsymbol{\gamma} \tag{18}$$

where $\boldsymbol{\sigma}$ is a positive definite shift matrix and ξ_σ is chosen such that the shifted Hessian $(\boldsymbol{\eta} - \xi_\sigma \boldsymbol{\sigma})$ is positive definite and the step size is reasonable. In geometry optimizations, the shift matrix is often taken to be the identity matrix for convenience, and the rational function optimization (RFO) method[20] is used to compute ξ_σ as the most negative eigenvalue of the augmented Hessian

$$\eta_{aug} = \begin{bmatrix} \boldsymbol{\eta} & \boldsymbol{\gamma} \\ \boldsymbol{\gamma}^T & 0 \end{bmatrix} \tag{19}$$

In some problems, such as those with strongly coupled coordinates or ill-conditioned Hessians, the use of the identity matrix can lead to numerical instabilities or slow convergence. A shift matrix that incorporates some of the coupling between coordinates and which has an eigenvalue spectrum that has a similar distribution of weakly and strongly coupled modes as

04 June 2025 14:14:31

the actual Hessian should better account for be a superior choice. Over the course of testing and implementing the VRC method, the overlap of the basis set derivatives was found to provide better optimization behavior than the identity matrix

$$\sigma_{i\mu j\nu} = \int_{t_R}^{t_P} \delta_{ij} \frac{d\phi_\mu}{dt} \frac{d\phi_\nu}{dt} dt \tag{20}$$

The augmented Hessian used to compute the shift parameter for the RFO method, may be constructed after scaling eqn 19 as follows

$$\eta_{aug,scaled} = \begin{bmatrix} \boldsymbol{\sigma} & 0 \\ 0 & 1 \end{bmatrix}^{-1/2} \begin{bmatrix} \boldsymbol{\eta} & \boldsymbol{\gamma} \\ \boldsymbol{\gamma}^T & 0 \end{bmatrix} \begin{bmatrix} \boldsymbol{\sigma} & 0 \\ 0 & 1 \end{bmatrix}^{-1/2} \tag{21}$$

When ξ_σ is initialized according to the RFO method, eqn 18 will produce a step towards the SDRP. If the predicted step is unreasonably large or the quadratic approximation to the current error $Q_\epsilon(\mathbf{C} + \mathbf{\Delta C})$ is less than zero, the magnitude of ξ_σ is increased until the step size is below a maximum allowed step size and the estimated error is greater than or equal to zero. $Q_\epsilon(\mathbf{C} + \mathbf{\Delta C})$ can be constructed by differentiating equation 3 with respect to a change in the LEC.

The unconstrained VRC optimization algorithm is as follows

1. Input initial path, maximum step size δ
2. Compute VRE, VRE derivatives, ϵ and $\boldsymbol{\sigma}$.
3. Set ξ_σ to the RFO eigenvalue using Hessian/gradient scaled by $\boldsymbol{\sigma}^{-1/2}$ as in eq 21
4. Compute displacement $\mathbf{\Delta C}$ by eq 18, if $|\mathbf{\Delta C}| \geq \delta$, update ξ_σ until $|\mathbf{\Delta C}| \leq \delta$
5. Compute Q_ϵ, if $Q_\epsilon \leq 0$, update ξ_σ until $Q_\epsilon = 0$.
6. Check $|\mathbf{\Delta C}|$ for convergence, stop iterations if converged
7. Update LEC, recompute VRE, VRE derivatives, ϵ and $\boldsymbol{\sigma}$.
8. Compare predicted change in energy to actual change in energy, and update δ accordingly.
9. Goto 3

04 June 2025 14:14:31

This algorithm is capable of producing final pathways with very little error, even with a small number of LEC per coordinate (see Figure 4, discussed in greater detail in Section IV). Throughout the optimization, steady progress is made in the direction of the final pathway; however, much of the improvement in the path appears to take place in the early steps, and there is a substantial portion of the optimization (ca. 50% of the total steps) where the shape of the path, as well as the VRE and the magnitude of the VRE gradient, do not appear to change by much until the last few optimization steps where the behavior of the optimization appears to exhibit quadratic convergence. This sort of optimization behavior suggests strongly that there are degrees of freedom in the LEC for which the VRE is invariant, and the algorithm needs to be modified to account for these degrees of freedom.

C. Constraints and constrained optimization

For a single pathway, there may be more than one set of LEC that closely describes the shape of a particular path in a given basis set. Since the VRE is a line integral which is invariant to the chosen representation of the pathway, these two sets of LEC will have approximately the same energy, and the value of both the first and the second derivative of the VRE in the direction of the displacement from one set to the other will be near zero.In an ideal optimization utilizing an infinite basis set and computing the VRE integrals exactly, these redundant coordinates would be pure and separable, and could be identified and eliminated at each iteration in order to accelerate and stabilize the convergence to the SDRP in much the same way as translation and rotation are removed from optimization of single geometries. With a finite basis set and numerical quadrature methods, however, such pure transformations do not necessarily exist, and the coupling between the redundant and non-redundant LEC can complicate the removal of the redundant coordinates from consideration.

In order to develop a more robust and reliable means to deal with the redundant degrees of freedom in the LEC, it is useful to begin by discussing these redundancies in the context of curve fitting. A parametric path $x(t)$ expressed as a linear combination of n basis functions that passes through a set of n geometries x_i can be found by solving a set of $n \times m$ equations $x(t_i) = x_i$ for the $n \times m$ LEC, where m is the dimensionality of the geometries x_i. This requires that values of t_i are assigned to each of the x_i. Figure 2 shows that for a finite number

04 June 2025 14:14:31

of points and basis functions, assigning different sets of t_i yields curves that pass through all of the points but have quite different shapes. In the unconstrained VRC problem, the shape of the path is determined by minimization of the VRE, and the extra degrees of freedom arise from the many choices of x_i, t_i pairs that will produce LEC that approximate that shape for a given choice of basis functions. Even though the VRC treats the path as an inherently continuous object, the stability of the optimization can be improved by constraining the relationship between a set of n x_i, t_i pairs. A convenient choice of constraint involves the arc length

$$S(t_1, t_2) = \int_{t_1}^{t_2} |\boldsymbol{\tau}(t)|\, dt \tag{22}$$

For n basis functions, the constraints on the t_i can easily be defined by dividing the path into $n+1$ segments, and specifying the ratios of the lengths of adjacent segments,

$$t_\alpha = \frac{\alpha}{n+1} \qquad 0 \leq \alpha \leq n+1 \tag{23}$$

$$S(t_{\alpha-1}, t_\alpha) = c_\alpha S(t_\alpha, t_{\alpha+1}) \qquad 1 \leq \alpha \leq n+1 \tag{24}$$

By making the c_α depend on properties of the path or PES, the flexibility of the basis set could be focused on the regions of large curvature or high relative energies that may be the most important for understanding the reaction. In the present work, however, the c_i are always chosen to be equal to 1 in order to maintain a uniform description of the path. This leads to n constraint functions

$$\kappa_\alpha(\mathbf{C}) = 0 = S(t_{\alpha-1}, t_\alpha) - S(t_\alpha, t_{\alpha+1}) \qquad 1 \leq \alpha \leq n \tag{25}$$

The method of Lagrange multipliers may be used to enforce these constraints during the minimization of the VRE

$$\mathcal{L}_{CVRC} = Q_{VRE}(\mathbf{C}) - \frac{1}{2}\xi_\sigma \Delta\mathbf{C}^{\mathrm{T}} \boldsymbol{\sigma} \Delta\mathbf{C} + \sum_\alpha \lambda_\alpha \kappa_\alpha(\mathbf{C}) \tag{26}$$

Equation 26 is the constrained VRC (CVRC) Lagrangian, where ξ_σ is the shift parameter chosen to ensure that a downhill step is taken that was used in the unconstrained method, and is computed using the same scaled RFO approach as before. The path may be updated iteratively towards the solution by requiring that $\mathcal{L}_{CVRC}$ is stationary with respect to a change in both the LEC and the multipliers λ_α

$$\frac{\partial \mathcal{L}}{\partial C} = 0 \text{ and } \frac{\partial \mathcal{L}}{\partial \lambda_\alpha} = \kappa_\alpha = 0 \qquad 1 \leq \alpha \leq n \tag{27}$$

04 June 2025 14:14:31

The integrals required to compute the terms in Q_{VRE} depend on the potential energy of the surface and therefore are computationally expensive to evaluate, while the integrals necessary to compute the κ_α and their derivatives with respect to a change in the LEC depend only on the evaluation of the basis functions and are relatively inexpensive. Since both Q_{VRE} and the κ_α have a strongly curvilinear dependence upon the LEC, it makes sense to solve for the $\mathbf{\Delta C}$ and λ_α using a microiterative approach for each evaluation of the VRE derivatives $\boldsymbol{\gamma}$ and $\boldsymbol{\eta}$. Because ξ_σ corrects $\boldsymbol{\eta}$, it is only recomputed once per macroiteration when $\boldsymbol{\gamma}$ and $\boldsymbol{\eta}$ are evaluated.

In addition to minimizing the VRE under the constraint that n points along the path remain uniformly spaced, it would be advantageous to also include terms to control step size and restrict the solution to displacements with predicted VRE error greater than zero. In order to do this, the following additional terms can be added to equation 26:

$$\frac{1}{2}\mu_\delta \left(\mathbf{\Delta C}^T \mathbf{\Delta C} - \delta^2\right) \tag{28}$$

$$\mu_\epsilon \boldsymbol{\epsilon} \left(\mathbf{C} + \mathbf{\Delta C}\right) \tag{29}$$

04 June 2025 14:14:31

where the μ are multipliers, δ is the maximum step size, and ϵ is the error as defined by equation 3, expanded as a quadratic Taylor series in $\mathbf{\Delta C}$ with the derivatives given by:

$$\frac{\partial \epsilon}{\partial C_{i\mu}} = \gamma_{i\mu} - 2g_i\left(\mathbf{x}\left(t_{ts}\right)\right)\phi_\mu\left(t_{ts}\right) \tag{30}$$

$$\frac{\partial^2 \epsilon}{\partial C_{i\mu}\partial C_{j\nu}} = \eta_{i\mu j\nu} - 2H_{ij}\left(\mathbf{x}\left(t_{ts}\right)\right)\phi_\mu\left(t_{ts}\right)\phi_\nu\left(t_{ts}\right) \tag{31}$$

The first term is not included in the Lagrangian unless the microiterations produce an LEC displacement with a magnitude that exceeds δ, while the second term is only included when the estimate of the error falls below zero. The derivatives of $\mathcal{L}_{CVRC}$ during each phase of

the microiterations are computed as follows:

$$\frac{\partial \mathcal{L}_{CVRC}}{\partial \mathbf{C}} = \boldsymbol{\gamma} + (\boldsymbol{\eta} - \xi_\sigma \boldsymbol{\sigma} + \mu_\delta \mathbf{I})\, \boldsymbol{\Delta C} + \sum_\alpha \lambda_\alpha \frac{\partial \kappa_\alpha (\mathbf{C} + \boldsymbol{\Delta C})}{\partial \mathbf{C}} + \mu_\epsilon \frac{\partial \epsilon_{VRC} (\mathbf{C} + \boldsymbol{\Delta C})}{\partial \mathbf{C}} \tag{32}$$

$$\frac{\partial \mathcal{L}_{CVRC}}{\partial \lambda_\alpha} = \kappa_\alpha \tag{33}$$

$$\frac{\partial \mathcal{L}_{CVRC}}{\partial \mu_\delta} = \frac{1}{2}\left(\boldsymbol{\Delta C}^T \boldsymbol{\Delta C} - \delta^2\right) \tag{34}$$

$$\frac{\partial \mathcal{L}_{CVRC}}{\partial \mu_\epsilon} = \epsilon (\mathbf{C} + \boldsymbol{\Delta C}) \tag{35}$$

$$\frac{\partial^2 \mathcal{L}_{cVRC}}{\partial \mathbf{C}^2} = \boldsymbol{\eta} - \xi_\sigma \boldsymbol{\sigma} + \mu_\delta \mathbf{I} + \sum_\alpha \lambda_\alpha \frac{\partial^2 \kappa_\alpha (\mathbf{C} + \boldsymbol{\Delta C})}{\partial \mathbf{C}^2} + \mu_\epsilon \frac{\partial^2 \epsilon_{VRC} (\mathbf{C} + \boldsymbol{\Delta C})}{\partial \mathbf{C}^2} \tag{36}$$

$$\frac{\partial^2 \mathcal{L}_{cVRC}}{\partial \mathbf{C} \partial \lambda_\alpha} = \frac{\partial \kappa_\alpha (\mathbf{C} + \boldsymbol{\Delta C})}{\partial \mathbf{C}} \tag{37}$$

$$\frac{\partial^2 \mathcal{L}_{cVRC}}{\partial \mathbf{C} \partial \mu_\delta} = \boldsymbol{\Delta C} \tag{38}$$

$$\frac{\partial^2 \mathcal{L}_{cVRC}}{\partial \mathbf{C} \partial \mu_\epsilon} = \frac{\partial \epsilon_{VRC} (\mathbf{C} + \boldsymbol{\Delta C})}{\partial \mathbf{C}} \tag{39}$$

$$\begin{pmatrix} \boldsymbol{\Delta C} \\ \boldsymbol{\Delta \lambda}_\kappa \\ \boldsymbol{\Delta \mu}_\delta \\ \boldsymbol{\Delta \mu}_\epsilon \end{pmatrix} = - \begin{pmatrix} \frac{\partial^2 \mathcal{L}}{\partial \mathbf{C}^2} & \frac{\partial^2 \mathcal{L}}{\partial \mathbf{C} \partial \boldsymbol{\lambda}_\kappa} & \frac{\partial^2 \mathcal{L}}{\partial \mathbf{C} \partial \mu_\delta} & \frac{\partial^2 \mathcal{L}}{\partial \mathbf{C} \partial \mu_\epsilon} \\ \frac{\partial^2 \mathcal{L}}{\partial \mathbf{C} \partial \boldsymbol{\lambda}_\kappa}^T & \mathbf{0} & \mathbf{0} & \mathbf{0} \\ \frac{\partial^2 \mathcal{L}}{\partial \mathbf{C} \partial \mu_\delta}^T & \mathbf{0} & \mathbf{0} & \mathbf{0} \\ \frac{\partial^2 \mathcal{L}}{\partial \mathbf{C} \partial \mu_\epsilon}^T & \mathbf{0} & \mathbf{0} & \mathbf{0} \end{pmatrix}^{-1} \begin{pmatrix} \frac{\partial \mathcal{L}}{\partial \mathbf{C}} \\ \frac{\partial \mathcal{L}}{\partial \boldsymbol{\lambda}_\kappa} \\ \frac{\partial \mathcal{L}}{\partial \mu_\delta} \\ \frac{\partial \mathcal{L}}{\partial \mu_\epsilon} \end{pmatrix} \tag{40}$$

The CVRC algorithm is as follows

1. Input initial path, maximum step size δ
2. Compute VRE, VRE derivatives, ϵ and $\boldsymbol{\sigma}$
3. Set ξ_σ to the RFO eigenvalue using Hessian/gradient scaled by $\boldsymbol{\sigma}^{-1/2}$ as in eq 21, set $\boldsymbol{\Delta C}$, $\boldsymbol{\lambda}_\kappa$, μ_δ and μ_ϵ to $\mathbf{0}$
4. Begin microiterations
   (a) Compute the constraints $\kappa (\mathbf{C} + \boldsymbol{\Delta C})$ and their derivatives w.r.t. a change in the LEC

04 June 2025 14:14:31

(b) Compute $\epsilon(\mathbf{C}+\mathbf{\Delta C})$ and $|\mathbf{\Delta C}|$ and turn on optimization of μ_δ and μ_ϵ if necessary

(c) Compute derivatives of the Lagrangian according to eqs 32-39

(d) Update $\mathbf{\Delta C}$, $\boldsymbol{\lambda}_\kappa$, μ_δ and μ_ϵ according to eq 40

(e) Check augmented gradient and augmented displacement for convergence of microiterations, end microiterations if converged

(f) goto 4a

5. Check $|\mathbf{\Delta C}|$ for convergence, and end macroiterations if converged

6. Update LEC for path, recompute VRE, VRE derivatives and ϵ

7. Compare predicted versus actual change in VRE, and update δ accordingly

8. goto 3

04 June 2025 14:14:31

The constrained VRC algorithm not only manages to get close to the IRC path in fewer iterations than the unconstrained algorithm, it also manages to achieve full convergence much more quickly. The primary drawback to using the constraints is that the flexibility in the LEC is reduced in order to satisfy the constraints, which results in a higher VRE at the final converged path than in the unconstrained case. Additionally, ξ_σ does not approach zero near convergence as it does in the unconstrained case. This is likely because it is computed using the unconstrained η which may not be positive definite, and the unconstrained γ which may be non-zero in the direction of the constraints. Early attempts to consider the constraints in the calculation of ξ_σ or to include the optimization of ξ_σ in the microiteration phase resulted in a loss of stability in the algorithm. It is possible that convergence may be accelerated near the solution by improved handling/computation of ξ_σ, and so future investigation is warranted.

Both the constrained and unconstrained algorithms have a tendency to slow down or produce poor step directions early on, when the path is in a region of the PES with incorrect curvature. This is an unfortunate consequence of the VRE's dependence on the gradient norm, as the gradient norm will also be small near higher order stationary points on the PES. This can also complicate the calculation of the VRE Hessian, since eq 13 becomes singular when the PES gradient goes to zero. These features can result in steps that are

unnecessarily small or cautious as the VRC method has a strong preference to avoid an increase in the gradient norm along the path even early in an optimization where it may be more sensible to focus on reducing the energy of the transition state. In the following section, a modification to the CVRC algorithm is outlined that couples together a standard transition state optimization step with the VRC path relaxation in order to improve the efficiency of the method when the path is far from convergence.

III. COMBINED PATH AND TRANSITION STATE OPTIMIZATION

A. TS Coupling constraints

Path optimization methods are often used to produce an approximate geometry corresponding to the transition state connecting two minimum energy structures, which is then further refined by saddle point optimization methods. Path optimization typically requires a significant number of potential energy surface evaluations to produce an approximate structure, but the resulting approximate structures tend to converge more rapidly and/or reliably to the transition state than simpler interpolation schemes like LST/QST[21,22], or local optimization methods like the dimer method[23]. Additionally, the converged path is usually sufficient to confirm that the transition state does connect the minimum energy structures, so further improvement of the path by reaction path following is not performed. In existing discrete path optimization methods, the approximation of a transition state geometry is usually accomplished either by interpolation between the highest energy structures following convergence of the path, or by treating the highest energy structure (typically called the *climbing* structure[24]) differently than the rest in order to allow it to loosely converge to the saddle point rather than an arbitrary point near the SDRP.

The VRC method expresses and optimizes the path as a single, continuous object, so producing a geometry to refine to the transition state following the VRC optimization would be a fairly trivial and straightforward optimization of the potential energy with respect to the parameter t. The second approach is less straightforward to adapt to the VRC method, and before discussing how this can be accomplished, it is worthwhile to consider what effect coupling a transition state optimization would have given the continuous description of the path. In a similar fashion to how a discrete path optimization assigns one point along the

04 June 2025 14:14:31

path to be a climbing structure, the coupling of a transition state optimization to the VRC method could be thought of as dedicating m of the LEC to the optimization of the transition state geometry. The path for a chemical system described by m coordinates and expanded in a basis of n functions has $m \times n$ degrees of freedom minus the n constraints described earlier. Requiring that the path passes through a particular point (i.e. $\mathbf{x}(t_{ts}) = \mathbf{x}_{ts}$) amounts to setting an additional m TS coupling constraints:

$$0 = \Delta_i x_{ts} = x_i(t_{ts}) - x_{ts,i} \qquad 1 \leq i \leq m \tag{41}$$

while introducing an extra degree of freedom in t_{ts}. The inclusion of t_{ts} as an extra degree of freedom highlights a significant benefit to using a continuous description of the path: the location of the transition state along the path is entirely independent of the representation of the path and the evaluation of the VRE or its derivatives, as well as the constraints from the previous section that define the relationship between the arc length and t.

As with the arc length constraints used in the previous section, the TS coupling constraints are enforced during the optimization through the use of Lagrange multipliers which are determined microiteratively. Each TS coupling constraint has two terms, the first of which, $x_i\left(t_{ts}\right)$, is the evaluation of coordinate i at the parameter value t_{ts} and therefore depends on the current value of the LEC during the microiterations (i.e. $\mathbf{C} + \mathbf{\Delta C}$). The second term $x_{ts,i}$ is the goal value of coordinate i for the transition state at this iteration of the optimization. This goal structure could be defined implicitly as a functional of the LEC, for example by using the predicted PES gradient or energy at $\mathbf{x}\left(t_{ts}\right)$, which would allow the goal structure to be updated during the microiterations. This approach could have some benefit, but the present discussion will be limited to an explicit definition of $\mathbf{x}_{ts}$, where the goal geometry is computed once per macroiteration using a modified Newton step on the PES from the highest energy point along the path for the current macroiteration and is considered to be fixed during the microiterative portion of the algorithm. This separation allows for the use of standard methods like step size control and line search on the more familiar chemical PES, rather than the VRE potential, and allows the transition state optimization to be viewed as a means to focus the VRC optimization toward a particular region of the PES that's more likely to contain the transition state, and therefore, the SDRP. For this reason, this approach will be referred to as the focused VRC (FVRC) method for the remainder of this paper.

04 June 2025 14:14:31

The method for computing the goal structure for the transition state is discussed in greater detail in section III B, but for now, let $\mathbf{\Delta x}$ be the m-dimensional array of TS coupling constraints defined as in eq 41. The FVRC Lagrangian is given below

$$\begin{aligned}\mathcal{L}_{FVRC} =& Q_{VRE}\left(\mathbf{C}+\mathbf{\Delta C}\right) - \frac{1}{2}\xi_{\sigma}\Delta\mathbf{C}^{\mathrm{T}}\boldsymbol{\sigma}\left(\mathbf{C}\right)\Delta\mathbf{C} + \mu_{\epsilon}\epsilon_{FVRC}\left(\mathbf{C}+\mathbf{\Delta C}\right) \\ &+ \sum_{\alpha}\lambda_{\alpha}\kappa_{\alpha}\left(\mathbf{C}+\mathbf{\Delta C}\right) + \left(\boldsymbol{\theta}+\frac{1}{2}\mathbf{\Delta x}\right)^{T}\mathbf{\Delta x} \end{aligned} \tag{42}$$

where the $\boldsymbol{\theta}$ are the multipliers for the TS coupling constraints. Aside from the addition of the TS coupling constraint term, there are changes to the step size and error terms compared to $\mathcal{L}_{CVRC}$. The step size term is dropped entirely since it may lead to an inconsistent Lagrangian if the LEC step size is too small to satisfy the TS coupling constraints, and is unnecessary since the transition state optimization has a controlled step size and limiting the step size of the transition state is sufficient to limit the change in the LEC. Recall that the error is defined as the VRE minus the projected VRE, and that the projected VRE is a sum of the forward and reverse energy barriers. So long as the TS coupling constraints are satisfied, the estimated projected VRE does not depend on the LEC and the FVRC error simplifies to

$$\epsilon_{FVRC}\left(\mathbf{C}+\mathbf{\Delta C}\right) = Q_{VRE}\left(\mathbf{C}+\mathbf{\Delta C}\right) - E_{ppVRE} \tag{43}$$

where E_{ppVRE} is the predicted projected VRE, evaluated using computed or estimated energies corresponding to the geometry updated by the transition state optimization step. Since E_{ppVRE} is constant with respect to a change in the LEC, its derivatives are equal to the derivatives of the VRE LQA. This approximation is only valid when the path passes through the updated geometry, so optimization of μ_{ϵ} should not be attempted unless the predicted error is less than zero *and* $|\mathbf{\Delta x}| = 0$. Another consequence of defining the error as being relative to the projected VRE of the final path is that the only term in $\mathcal{L}_{FVRC}$ that depends on t_{ts} is the TS coupling constraint term. As a notational convenience, let the TS coupling constraint term be $\mathcal{F} = \left(\boldsymbol{\theta}+\frac{1}{2}\mathbf{\Delta x}\right)^{T}\mathbf{\Delta x}$. The derivatives of $\mathcal{F}$ with respect to a change in the LEC, the coupling constraint multipliers $\boldsymbol{\theta}$, and t_{ts} are derived

04 June 2025 14:14:31

straightforwardly:

$$\frac{\partial \mathcal{F}}{\partial \theta_i} = \Delta_i x_{ts} \tag{44}$$

$$\frac{d\mathcal{F}}{dt_{ts}} = (\boldsymbol{\theta} + \boldsymbol{\Delta}\mathbf{x})^T \boldsymbol{\tau}(t_{ts}) \tag{45}$$

$$\frac{\partial \mathcal{F}}{\partial C_{i\mu}} = (\theta_i + \Delta_i x_{ts}) \phi_\mu(t_{ts}) \tag{46}$$

$$\frac{d\partial \mathcal{F}}{dt_{ts}\partial \theta_i} = \tau_i(t_{ts}) \tag{47}$$

$$\frac{d^2\mathcal{F}}{dt_{ts}^2} = (\boldsymbol{\theta} + \boldsymbol{\Delta}\mathbf{x})^T \frac{d\boldsymbol{\tau}(t_{ts})}{dt} + \boldsymbol{\tau}(t_{ts})^T \boldsymbol{\tau}(t_{ts}) \tag{48}$$

$$\frac{d\partial \mathcal{F}}{dt_{ts}\partial C_{i\mu}} = \tau_i(t_{ts}) \phi_\mu(t_{ts}) + (\theta_i + \Delta_i x_{ts}) \frac{d\phi_\mu(t_{ts})}{dt} \tag{49}$$

$$\frac{\partial^2 \mathcal{F}}{\partial C_{i\mu}\partial \theta_j} = \delta_{ij} \phi_\mu(t_{ts}) \tag{50}$$

$$\frac{\partial^2 \mathcal{F}}{\partial C_{i\mu}\partial C_{j\nu}} = \delta_{ij} \phi_\mu(t_{ts}) \phi_\nu(t_{ts}) \tag{51}$$

B. Geometry optimization

As mentioned earlier, the difficulty in transition state optimization is a result of the requirement that the energy must be a maximum along the transition vector, while being a minimum in all other degrees of freedom. Not only is the selection of the transition vector difficult when far from the converged structure, but methods, like line searches, which are commonly used to accelerate the convergence of minimum energy structures cannot be used as there is no suitable metric to search. Since the energy must be a maximum in one direction, a search for the local minimum in the direction of the step may not be optimal. Likewise,when the curvature of the Hessian is incorrect, a search for the local minimum of the gradient norm or gradient squared in the direction of the step may not be optimal as these quantities may need to increase to move closer to the region of the PES containing the transition state. One additional benefit of the focused VRC method is that it turns the difficult problem of computing a step towards a transition state into the much simpler problem of computing a step that minimizes the energy from the current maximum along the path, allowing for the use of line searches to further accelerate convergence.

Since t_{ts} corresponds to the maximum along the current path, and since the maximum along the current path must be greater than or equal to the energy of the converged path,

04 June 2025 14:14:31

there is no need to select an eigenvector to be the transition vector when computing $\mathbf{x}_{ts}$. If the PES Hessian $\mathbf{H}_0$ at $\mathbf{x}_0 = \mathbf{x}(t_{ts})$ has the correct number of negative eigenvalues (one for a transition state), the corresponding eigenvector must be the transition vector and scaled Newton steps should suffice to converge to the transition state:

$$\mathbf{x}_{TS} = \mathbf{x}_0 - a_{scl}\mathbf{H}_0^{-1}\mathbf{g}_0 \tag{52}$$

where $\mathbf{g}_0$ is the gradient at $\mathbf{x}_0$ and a_{scl} is a scale factor which will be discussed later. If $\mathbf{H}_0$ has more than one negative eigenvalue or produces a step larger than the allowed step size with a_{scl}, a downhill step orthogonal to the tangent $\boldsymbol{\tau}$ of current path, is used instead:

$$\mathbf{P}_\tau^{\parallel} = \frac{\boldsymbol{\tau}\boldsymbol{\tau}^T}{\boldsymbol{\tau}^T\boldsymbol{\tau}}; \qquad \mathbf{P}_\tau^{\perp} = \mathbf{I} - \mathbf{P}_\tau^{\parallel} \tag{53}$$

$$\mathbf{x}_{TS} = \mathbf{x}_0 - a_{scl}\left(\mathbf{P}_\tau^{\perp}\mathbf{H}_0\mathbf{P}_\tau^{\perp} - \xi_{rfo}\mathbf{I} + \mathbf{P}_\tau^{\parallel}\right)^{-1}\mathbf{P}_\tau^{\perp}\mathbf{g}_0 \tag{54}$$

Since the step must lower the PES energy, regardless of how its computed, a line search may be employed to improve the quality of the goal structure. To carry out the line search, an $\mathbf{x}_1$ is computed according to eqn 54 or eqn 52 with $a_{scl} = a_1 \leq 1$ set so that $|\Delta\mathbf{x}| = |\mathbf{x}_1 - \mathbf{x}_0| \leq \delta_{max}$, where δ_{max} is the maximum allowed stepsize for the transition state. A fourth-order polynomial

$$p(\alpha) = c_0 + c_1\alpha + c_2\alpha^2 + c_3\alpha^3 + c_4\alpha^4 \tag{55}$$

can be constructed by using the energies $p(0) = V_0$ and $p(1) = V_1$ and the scalar gradients $p'(0) = \mathbf{g}_0^T\Delta\mathbf{x}$ and $p'(1) = \mathbf{g}_1^T\Delta\mathbf{x}$ as well as a constraint that there is only one minimum ($p''(\alpha) \geq 0$, see reference[25] for further details). This polynomial can be easily searched for the local minimum α_{min}. In the case where such a polynomial does not exist, instead of using a cubic fit as in the previous reference, a quartic polynomial with a zero cubic term $c_3 = 0$ is constructed instead. This polynomial will have more than one local minimum, and α_{min} is defined as the one closest to $\alpha = 1$. Once α_{min} is known, $\mathbf{x}_{TS}$ is updated using $a_{scl} = a_1\alpha_{min}$.

C. Handling rotations

One of the more attractive features of the VRC method is that no extra considerations need to be made for handling overall translation or rotation when working with Cartesian

04 June 2025 14:14:31

coordinates, which can improve the results of discrete path optimization[26]. By definition, an infinitesimal translation or rotation of the geometry at any point along the path will not change the magnitude of the gradient of the internal energy of evaluated at that point. It will, however, change the overall distance the path needs to travel from reactant to product. Because of this, minimization of the VRE will also minimize the overall translation and rotation contained in the path. Unfortunately, the same cannot be said about the TS coupling constraints defined in eqn 41.

Translation may be easily accounted for by requiring that the reactant and product both be *mean centered* by translating the atoms so that the average position of the x, y and z coordinate of the atoms in each structure are all zero. Rotation is a bit more difficult, as the goal structure is always defined in a particular rotational orientation, which may not necessarily be the optimal rotational orientation to minimize the VRE of a path that passes through the internal coordinates for that point. Extra care must be taken to limit the impact that the rotational orientation of the goal structure has on the relaxation of the path.

A projection method can be used to eliminate any translation or rotation from the TS geometry optimization step

$$\mathbf{P}_{TR} = \sum_{i}^{3} \frac{1}{n_{atoms}} \mathbf{t}_i \mathbf{t}_i^T + \mathbf{r}_i \left(\sum_{j}^{3} \mathbf{r}_j^T \mathbf{r}_j \right)^{-1} \mathbf{r}_i^T \tag{56}$$

where the portion of these vectors corresponding to the kth atom are given by

$$\mathbf{t}_{i,k} = \mathbf{e}_i \tag{57}$$

$$\mathbf{r}_{i,k} = \mathbf{x}_k \times \mathbf{e}_i \tag{58}$$

where $\times$ denotes the 3-dimesional cross product, $\mathbf{e}_i$ is the ith row of the 3-dimensional identity matrix, and $\mathbf{x}_k$ are the 3-dimensional Cartesian coordinates for atom k translated so that $\sum_k x_{k,i} = 0$ for each i. Constructed in this fashion, $\mathbf{P}_{TR}$ is a projection matrix onto the space of infinitesimal translation/rotations for the geometry given by $\mathbf{x}$, and by construction $\mathbf{P}_{TR}\mathbf{g} = 0$ when $\mathbf{P}_{TR}$ and $\mathbf{g}$ are computed at the same geometry. To eliminate the translation and rotation from a geometry optimization step, the Hessian and tangent may be modified in the following way prior to computing the step according to eqns 52-54

$$\mathbf{H}_{prj} = (\mathbf{I} - \mathbf{P}_{TR})\, \mathbf{H}_0\, (\mathbf{I} - \mathbf{P}_{TR}) + \mathbf{P}_{TR} \tag{59}$$

$$\boldsymbol{\tau}_{prj} = (\mathbf{I} - \mathbf{P}_{TR})\, \boldsymbol{\tau} \tag{60}$$

04 June 2025 14:14:31

This ensures that $\mathbf{x}_{TS}$ has no initial rotation relative to $\mathbf{x}(t_{TS})$ prior to the microterations. At every step of the microiterations, though, $\mathbf{x}_{TS}$ will need to be rotated to remove the overall rotation relative to the current value of $\mathbf{x}(t_{ts})$, and this can be done in the same fashion used to minimize the overall rotation of the product relative to the reactant.

D. Multiple Extrema

Up until this point, the discussion has assumed that the SDRP has exactly one transition state. If there are one or more intermediate minima with a corresponding number of additional transition states, it is a trivial matter to update the appropriate equations involving the error by using the more general form of the E_{pVRE} in equation 2 wherever appropriate. Additionally, for the FVRC method, each additional minima/TS pair adds another $2m$ constraints and 2 optimizable values of t. As long as there are sufficient LEC per coordinate (at least 2 or 3 per coupled structure appears to be sufficient), any number of additional geometry optimizations may be coupled to the VRE minimization. However, for unconverged paths, some care must be taken to distinguish between actual transition states, and maxima that are a result of the approximate path passing through a higher energy region of the PES rather than following the valley floor. This sort of maxima will occur when the path climbs the wall of the PES. Optimization steps computed at these false maxima and their associated minima may step towards the same stationary points as one of the actual maxima/minima optimizations. This can introduce a great deal of numerical instability into the microiterations or even result in an inconsistent FVRC Lagrangian, and should be avoided.

At each macroiteration of the VRC method, all of the local minima and maxima along the path are determined. If there are multiple maxima, the projection of the Hessian onto the tangent $\left(\boldsymbol{\tau}^T\mathbf{H}\boldsymbol{\tau}\right)$ at each maxima can be computed to determine if the energy along the path is maximized due to the curvature of PES (i.e. $\boldsymbol{\tau}^T\mathbf{H}\boldsymbol{\tau}$ is less than zero). Only these maxima are included in the microiteration phase of the current VRC macroiteration. When $\boldsymbol{\tau}^T\mathbf{H}\boldsymbol{\tau}$ is positive, optimization steps from the corresponding false maxima and the adjacent minima that's closest to it in energy are not included in the microiterations, and the minimization of the VRE should be sufficient to eliminate the false maxima/minima in subsequent optimization steps.

04 June 2025 14:14:31

E. FVRC algorithm

1. Input initial path
2. Compute VRE, VRE derivatives, ϵ, and $\boldsymbol{\sigma}$.
3. Locate and verify the t_e corresponding to the extrema (maxima and minima, or the transition states and intermediates) along the current path, and compute the $\mathbf{x}_e$ according to the methods in section III B.
4. Set ξ_σ to the RFO eigenvalue using Hessian/gradient scaled by $\boldsymbol{\sigma}^{-1/2}$ as in eq 21, set $\boldsymbol{\Delta C}$, $\boldsymbol{\lambda}_\kappa$, $\boldsymbol{\theta}$ and μ_ϵ to $\mathbf{0}$
5. Begin microiterations
   (a) Compute the constraints $\kappa\left(\mathbf{C}+\boldsymbol{\Delta C}\right)$ and their derivatives w.r.t. a change in the LEC
   (b) Rotate the $\mathbf{x}_e$ to remove the overall rotation relative to the current value of $\mathbf{x}\left(t_e\right)$, and compute $\boldsymbol{\Delta x}_e$
   (c) Compute $\epsilon\left(\mathbf{C}+\boldsymbol{\Delta C}\right)$ and turn on optimization of μ_ϵ if $\epsilon<0$ and $|\boldsymbol{\Delta x}| \approx 0$
   (d) Compute derivatives of the FVRC Lagrangian
   (e) Update $\boldsymbol{\Delta C}$, $\boldsymbol{\lambda}_\kappa$, $\boldsymbol{\theta}$, t_e and μ_ϵ
   (f) Check augmented gradient and augmented displacement for convergence of microiterations, end microiterations if converged
   (g) goto 5a
6. Update LEC for path, recompute VRE, VRE derivatives and ϵ.
7. Locate and verify the t_e corresponding to the extrema along the current path, and compute the $\mathbf{x}_e$
8. Check the gradient at the $\mathbf{x}_e$ for convergence, and end macroiterations if converged.
9. goto 4

04 June 2025 14:14:31

IV. RESULTS AND DISCUSSION

The methods described above were implemented in Mathmatica[27]. To illustrate the behavior of the VRC methods, two analytical potential energy surfaces will be used. The first is the analytical surface of Mller and Brown[28], multiplied by a scaling a factor of 1/627.52 so that the all of the unitless energies and displacements discussed below will more closely resemble atomic units than kcal/mol. This is a 2D surface that is frequently used in the development of new methods; though it is deceptively simple, it contains features such as combinations of soft and stiff vibrational modes and transition states with very small basins of attraction, both of which can cause difficulties for reaction path following/optimization methods. The VRC optimizations carried out on the Mller-Brown surface used a basis set with 9 optimizable LEC per coordinate, and the third derivatives of the PES necessary for evaluating the VRE Hessian (see eqn 13) were computed analytically. The line integrals for the VRE and its derivatives were evaluated by an adaptive integrator which computes the integral on a grid, and subdivides any interval with an unacceptable error estimate. The integrals were considered converged when the absolute maximum error for each interval was less than 10^{-8}, or the absolute relative error was less than 10^{-6} times the value of the integral. Since the focused VRC method requires the integration over regions of the PES where the gradient is very close to zero, an additional termination criteria was added: the maximum number of allowed subdivisions was set to 20; if this number is exceeded, the unconverged interval is ignored (its contribution to the quadrature is set to 0). This stopping criteria was never met in the evaluation of the integrals during the unconstrained or constrained optimizations.

The stopping criteria for the unconstrained VRC and constrained VRC algorithms were a computed RMS change to the LEC of less than 10^{-6}. The UVRC method converged in 54 iterations, with a final VRE only 1.2×10^{-6} higher than the VRE of the IRC. The CVRC required only 19 iterations to converge, but the final VRE was much higher at 6.0×10^{-3} over the IRC VRE. The FVRC method uses the convergence of the intermediates and transition states as a stopping criteria, and is considered converged when the RMS of the gradient at all intermediates and transition states is less than 10^{-6}. The FVRC method converges even more quickly than the CVRC method, requiring only 5 iterations, with a final VRE of 1.1×10^{-2} over the IRC VRE, which is an error of approximately 4%. To help put these

04 June 2025 14:14:31

VRE errors in context, the converged pathways are plotted alongside the IRC pathway in Figure 3. The UVRC pathway is nearly indistinguishable from the IRC as the full flexibility of the basis set is used to approximate the IRC, but both the CVRC and FVRC pathways still closely follow the IRC while cutting corners in a few places.

Figure 4 plots (a) the convergence of the VRE gradient, (b) LEC displacement and (c) PES gradient at the intermediates and transition states. The constraints in the CVRC and FVRC methods keep the VRE gradient from decreasing significantly even at convergence, as expected, but also demonstrates the difficulty of the UVRC optimization. By approximately iteration 25, the UVRC pathway is already lower in energy than either of the converged CVRC or FVRC, but it takes another 25 iterations for the path to find the correct parameterization to converge. The final few iterations demonstrate quadratic convergence behavior, as one would expect with a Newton-like method. The PES gradient plot demonstrates the efficiency and appeal of the FVRC method, as the intermediates and transition states are quickly determined along with an approximation to the SDRP. Figure 5 shows that path at each iteration of the FVRC method, demonstrating that the transition state and intermediate that are located near the initial path are quickly converged, and the remaining steps of the optimization are spent determining the location of the remaining transition state.

To demonstrate the performance of the FVRC method on a higher dimensional surface that is more representative of a chemical reaction, a 10-atom Lennard-Jones cluster[29] is used. In order to challenge the VRC method, the Cambridge cluster database[30] was consulted to locate two minimum structures which were known to be separated by two or more intermediates, with the 35th and 46th lowest energy structures satisfying that requirement. In anticipation of more intermediates and transition states, a basis set with 450 LEC (30 Cartesian coordinates expanded by 15 basis functions) was used, and the term in equation 13 corresponding to the third derivative of the PES was not included in the evaluation of the VRE Hessian as it was found to be unnecessary for good performance when using the FVRC method. The FVRC manages to converge to a pathway containing 4 intermediates and 5 transition states in 13 iterations, with a final VRE roughly 25% higher than the IRC VRE. Figure 6 shows the convergence of the VRE and PES gradients, and Figure 7 the energy along the pathway for selected iterations. By the 7th iteration, the energy profile along the path closely resembles the final energy.

04 June 2025 14:14:31

V. SUMMARY

The Variational Reaction Coordinate method provides a novel approach to the optimization of reaction pathways. By representing the pathway using a linear expansion in a continuous basis set, the line integral of the gradient norm and its derivatives with respect to a change in the linear expansion coefficients provides a foundation for constructing an iterative and variational algorithm for improving the approximation to a steepest descent reaction pathway. Additionally, constraints to fix the relationship between the basis function parameter t and the arc length traveled by the path, as well as constraints to couple the minimization of the variational reaction energy to the minimization of one or more points along the path (corresponding to intermediates and transition states), are described. Algorithms employing these constraints are able to rapidly determine the fully-converged structure of intermediates and transition states, as well as provide a good approximation to the reaction path.

The methods described in this paper achieve this rapid convergence at the expensive of a high per-iteration computational cost due to the necessity of using numerical methods to evaluate integrals that depend on the PES and its derivatives. In order for this method to enjoy routine use in the study of reactions using accurate Hartree Fock and Density Functional Theory energies, alternative means to evaluate the necessary integrals must be developed to reduce the per-iteration cost to something comparable to existing ad-hoc path optimization methods. These methods will be introduced and discussed in a future paper.

04 June 2025 14:14:31

VI. ACKNOWLEDGEMENT

This work was supported by grants from the National Science Foundation (CHE1212281, CHE1464450). We thank Wayne State University's computing grid for computer time.

REFERENCES

[1]K. Fukui, "The path of chemical reactions-the IRC approach," Acc. Chem. Res. **14**, 363–368 (1981).

[2]H. B. Schlegel, "Geometry optimization," WIREs Comput. Mol. Sci. **1**, 790–809 (2011).

[3]R. Elber and M. Karplus, "A method for determining reaction paths in large molecules: application to myoglobin," Chem. Phys. Lett. **139**, 375–380 (1987).

[4]G. Mills and H. Jónsson, "Quantum and thermal effects in H_2 dissociative adsorption: Evaluation of free energy barriers in multidimensional quantum systems," Phys. Rev. Lett. **72**, 1124 (1994).

[5]P. Y. Ayala and H. B. Schlegel, "A combined method for determining reaction paths, minima, and transition state geometries," J. Chem. Phys. **107**, 375–384 (1997).

[6]G. Henkelman and H. Jónsson, "Improved tangent estimate in the nudged elastic band method for finding minimum energy paths and saddle points," J. Chem. Phys. **113**, 9978–9985 (2000).

[7]W. E, W. Ren, and E. Vanden-Eijnden, "String method for the study of rare events," Phys. Rev. B **66**, 052301 (2002).

[8]B. Peters, A. Heyden, A. T. Bell, and A. Chakraborty, "A growing string method for determining transition states: Comparison to the nudged elastic band and string methods," J. Chem. Phys. **120**, 7877–7886 (2004).

[9]S. K. Burger and W. Yang, "Quadratic string method for determining the minimum-energy path based on multiobjective optimization," J. Chem. Phys. **124**, 054109 (2006).

[10]I. V. Khavrutskii, K. Arora, and C. L. Brooks III, "Harmonic Fourier beads method for studying rare events on rugged energy surfaces," J. Chem. Phys. **125**, 174108 (2006).

[11]A. Behn, P. M. Zimmerman, A. T. Bell, and M. Head-Gordon, "Incorporating linear synchronous transit interpolation into the growing string method: algorithm and applications," J. Chem. Theory Comput. **7**, 4019–4025 (2011).

[12]M. U. Bohner, J. Meisner, and J. Kästner, "A quadratically-converging nudged elastic band optimizer," J. Chem. Theory Comput. **9**, 3498–3504 (2013).

[13]P. Plessow, "Reaction path optimization without NEB springs or interpolation algorithms," J. Chem. Theory Comput. **9**, 1305–1310 (2013).

[14]P. M. Zimmerman, "Single-ended transition state finding with the growing string method," J. Comput. Chem. **36**, 601–611 (2015).

[15]R. Crehuet and J. M. Bofill, "The reaction path intrinsic reaction coordinate method and the Hamilton–Jacobi theory," J. Chem. Phys. **122**, 234105 (2005).

[16]A. Aguilar-Mogas, R. Crehuet, X. Giménez, and J. M. Bofill, "Applications of analytic and geometry concepts of the theory of calculus of variations to the intrinsic reaction

04 June 2025 14:14:31

coordinate model," Mol. Phys. **105**, 2475–2492 (2007).

[17]W. Quapp, "Chemical reaction paths and calculus of variations," Theor. Chem. Acc. **121**, 227–237 (2008).

[18]C. de Boor, *A practical guide to splines* (Springer-Verlag New York, 1978).

[19]R. B. Dash and D. Das, "A mixed quadrature rule by blending Clenshaw-Curtis and Gauss-Legendre quadrature rules for approximation of real definite integrals in adaptive environment," in *Proceedings of the International Multi–Conference of Engineer and Computer Scientists*, Vol. 1 (2011).

[20]A. Banerjee, N. Adams, J. Simons, and R. Shepard, "Search for stationary points on surfaces," J. Phys. Chem. **89**, 52–57 (1985).

[21]C. Peng and H. B. Schlegel, "Combining synchronous transit and quasi-newton methods to find transition states," Isr. J. Chem. **33**, 449–454 (1993).

[22]T. A. Halgren and W. N. Lipscomb, "The synchronous-transit method for determining reaction pathways and locating molecular transition states," Chem. Phys. Lett. **49**, 225–232 (1977).

[23]G. Henkelman and H. Jonsson, "A dimer method for finding saddle points on high dimensional potential surfaces using only first derivatives," J. Chem. Phys. **111**, 7010 (1999).

[24]G. Henkelman, B. P. Uberuaga, and H. Jónsson, "A climbing image nudged elastic band method for finding saddle points and minimum energy paths," J. Chem. Phys. **113**, 9901–9904 (2000).

[25]H. B. Schlegel, "Optimization of equilibrium geometries and transition structures," J. Comput. Chem. **3**, 214–218 (1982).

[26]M. Melander, K. Laasonen, and H. Jónsson, "Removing external degrees of freedom from transition-state search methods using quaternions," J. Chem. Theory Comput. **11**, 1055–1062 (2015).

[27]"Mathematica version 9.0," Wolfram Research, Inc. Champaign, IL (2013).

[28]K. Müller and L. D. Brown, "Location of saddle points and minimum energy paths by a constrained simplex optimization procedure," Theor Chim Acta **53**, 75–93 (1979).

[29]J. E. Lennard-Jones, "On the determination of molecular fields." Proc. Roy. Soc. A **106**, 441–462 (1924).

[30]D. Wales, J. Doye, A. Dullweber, M. Hodges, F. Naumkin, F. Calvo, J. Hernández-Rojas, and T. Middleton, "The Cambridge Cluster Database," URL

04 June 2025 14:14:31

http://doye.chem.ox.ac.uk/networks/LJn.html (2002).

04 June 2025 14:14:31

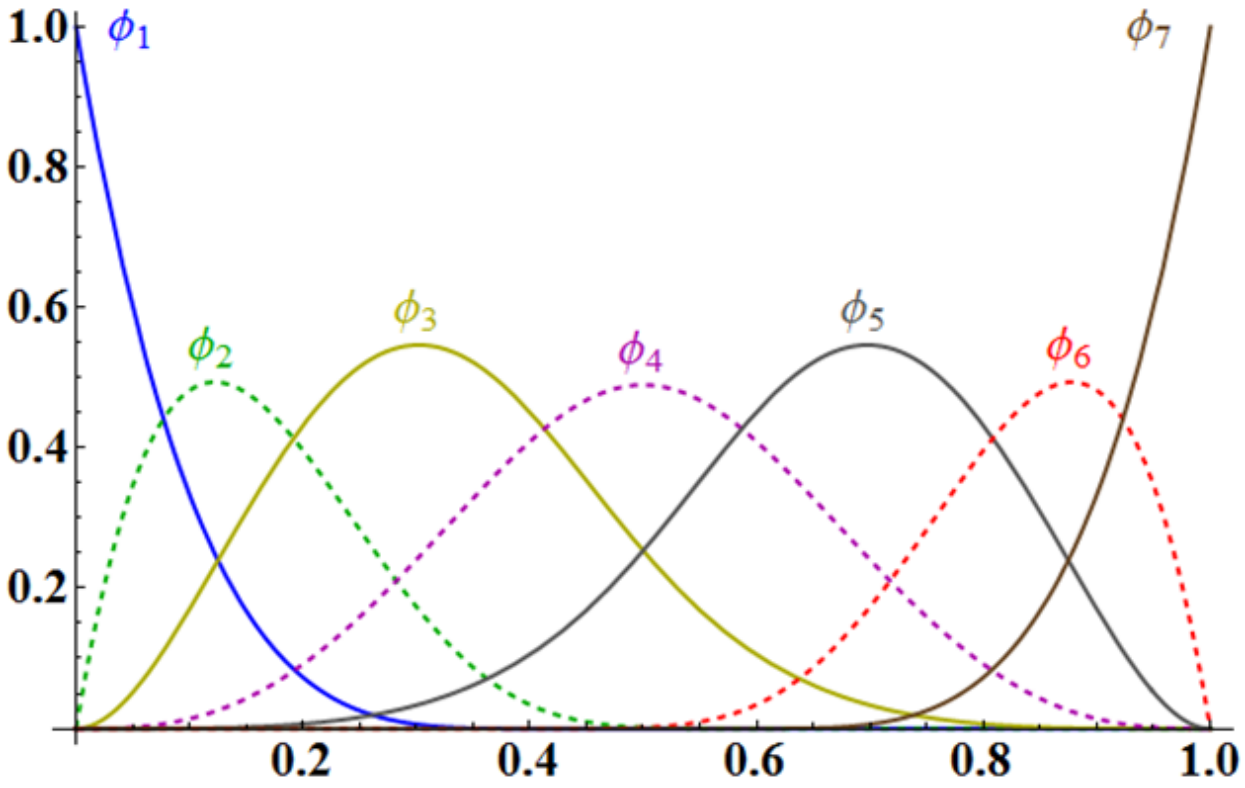

FIG. 1. B-Spline basis with 5 internal functions ($\phi_2 - \phi_7$) and 2 capping functions (ϕ_1 and ϕ_7)

04 June 2025 14:14:31

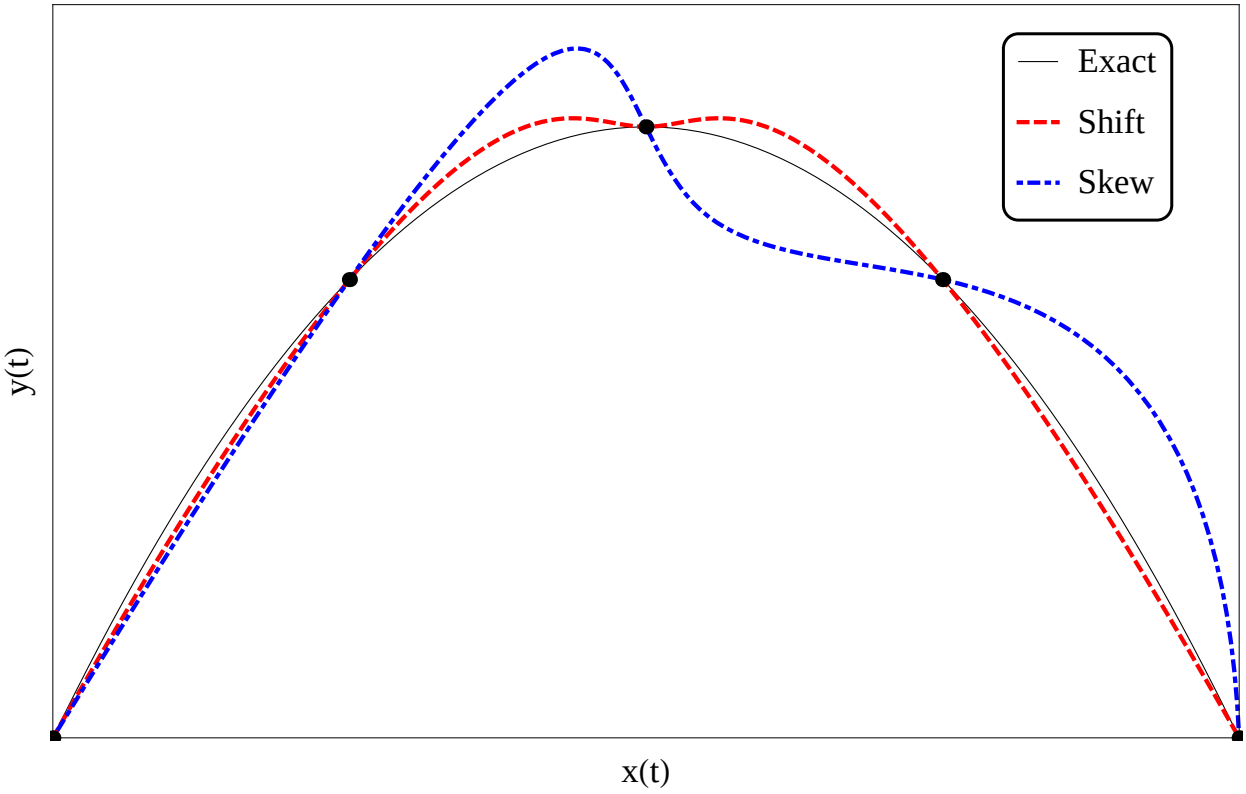

FIG. 2. Three cubic spline curves fit to the same 5 x,y pairs, using different values of t. Exact t = (0,0.25,0.5,0.7,1), Shift t = (0,0.15,0.5,0.85,1), Skew t = (0,0.1,0.4,0.7,1)

04 June 2025 14:14:31

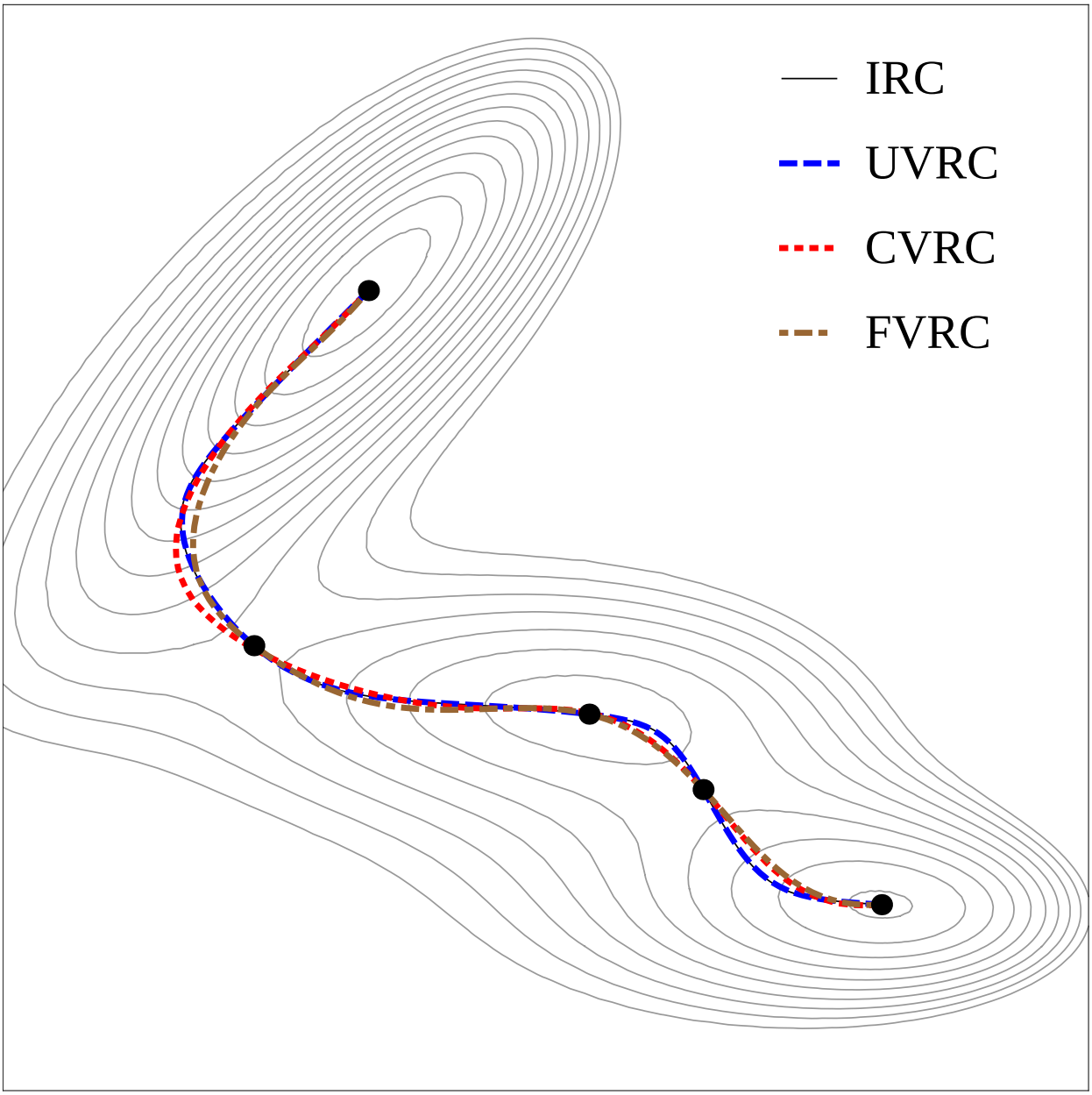

FIG. 3. Comparison of the shape of the converged unconstrained VRC (UVRC), constrained VRC (CVRC) and focused VRC (FVRC) pathways on the Mller-Brown analytical surface. The solid curve is the IRC, and the large dots are the minima and transition states along the IRC.

04 June 2025 14:14:31

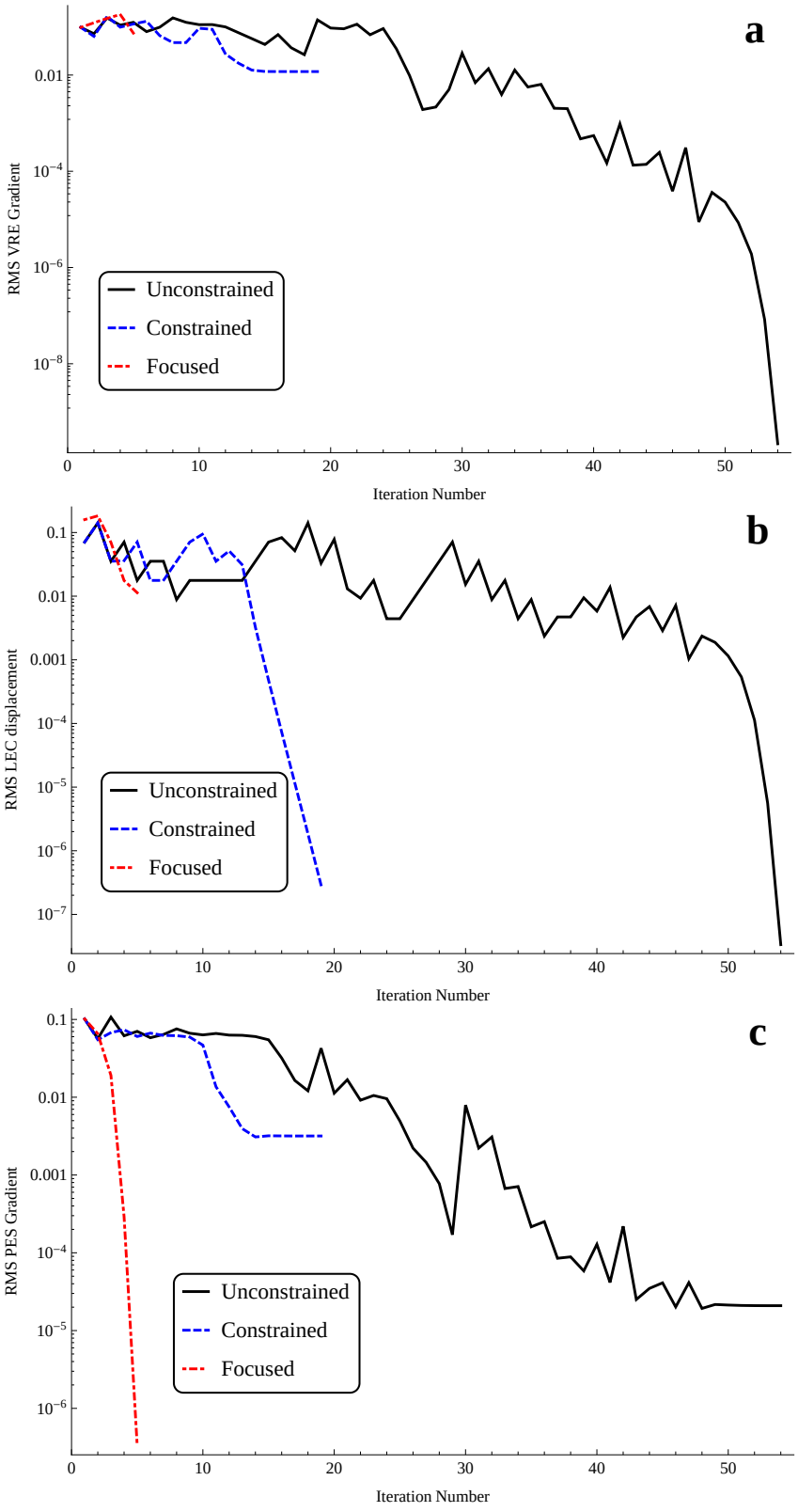

FIG. 4. Convergance log plots for the various VRC methods on the Mller-Brown surface. (a) RMS VRE gradient (b) RMS LEC displacement (c) RMS PES gradient (evaluated at the minima and maxima along the path only)

04 June 2025 14:14:31

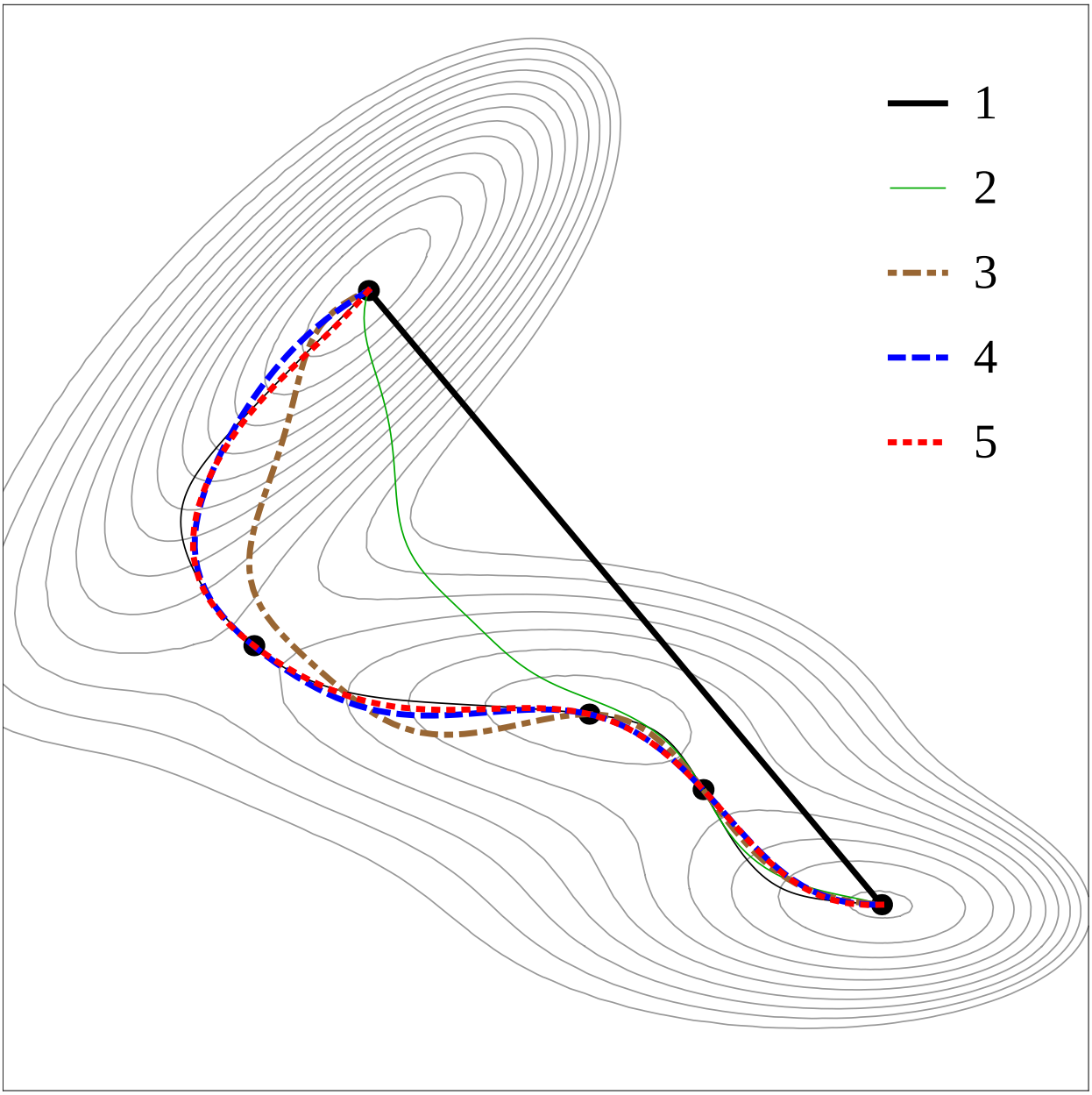

FIG. 5. The paths at every iteration of the FVRC method on the Mller-Brown surface, compared with the IRC.

04 June 2025 14:14:31

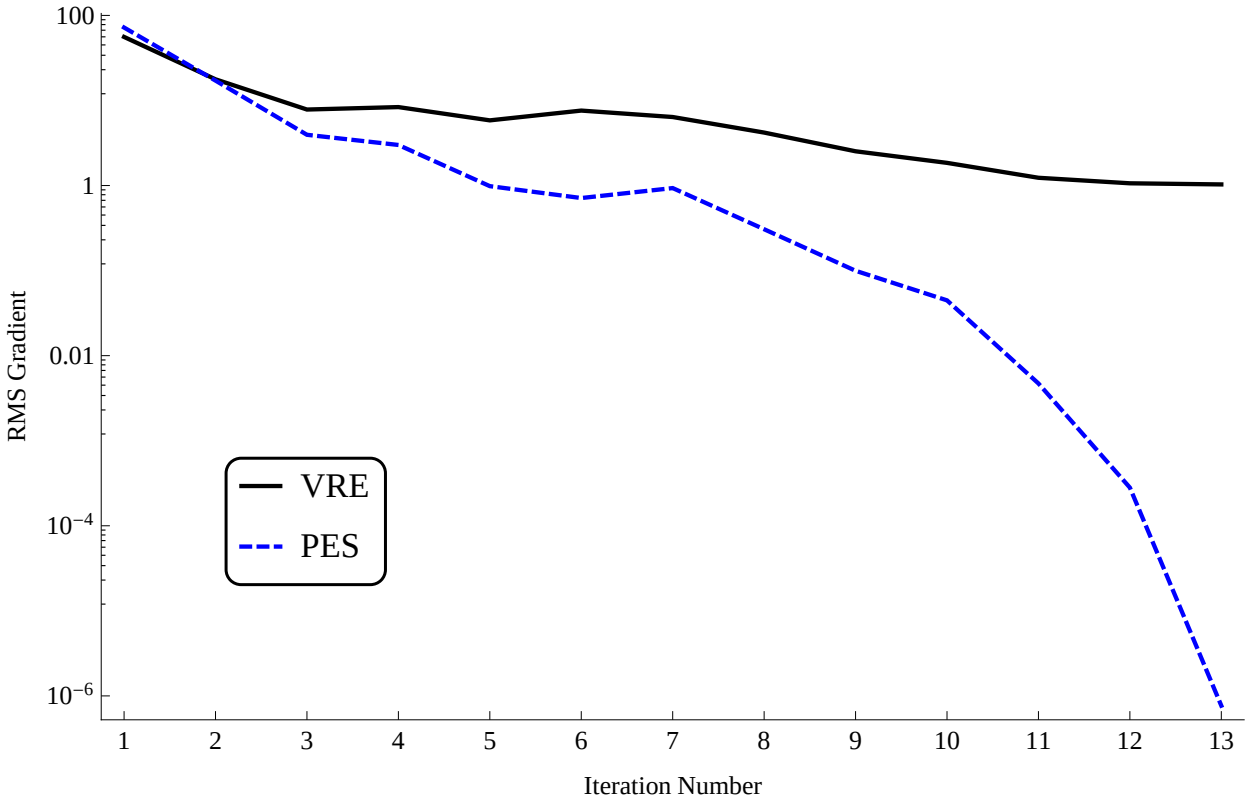

FIG. 6. Convergence of the VRE and PES gradient using the FVRC method on the LJ10 surface.

04 June 2025 14:14:31

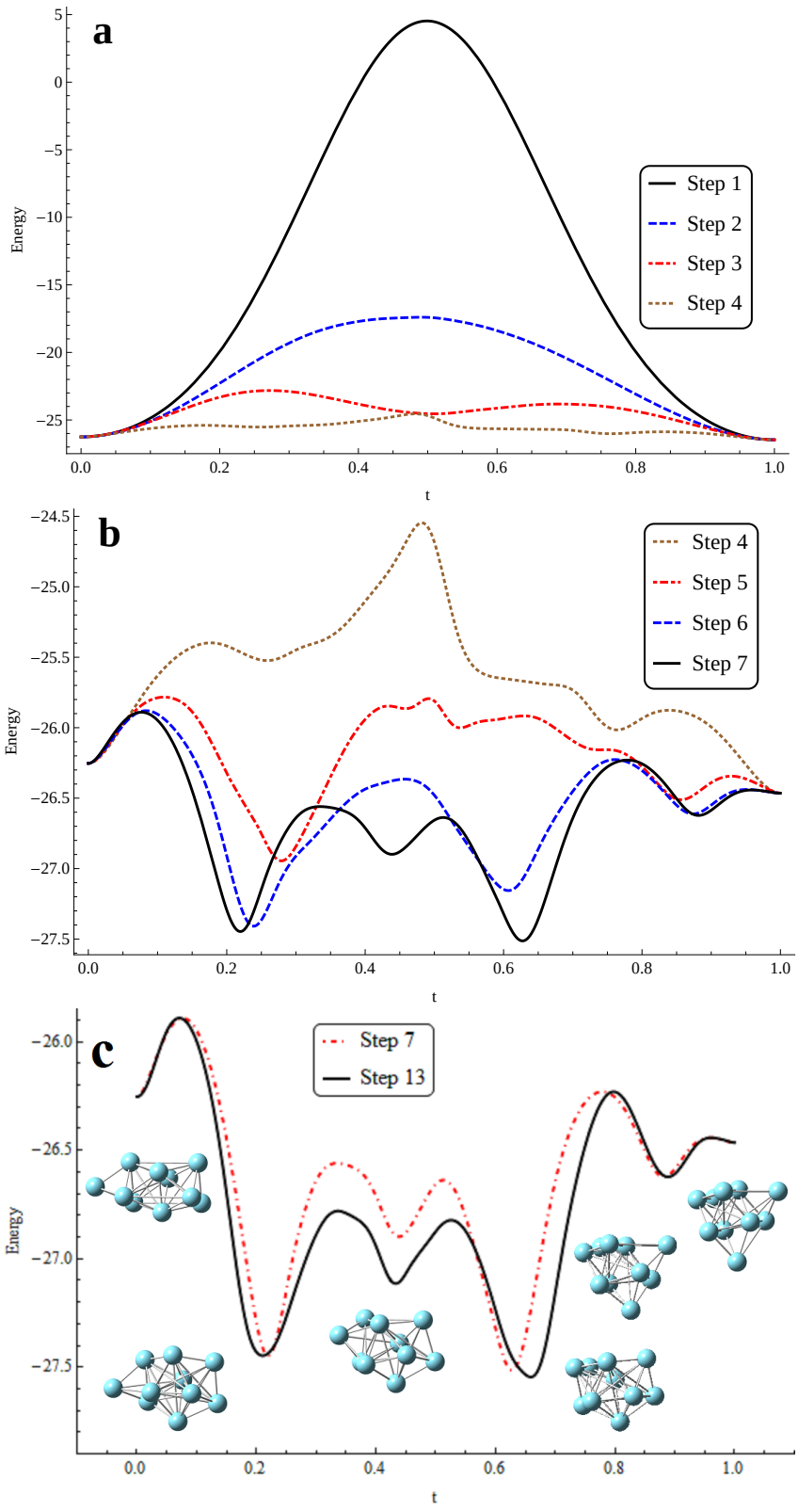

FIG. 7. Energy plots for selected iterations of the LJ10 FVRC optimization. (a) Iterations 1-4 (b) Iterations 4-7 (c) Comparison of the 7th and final (13th) steps, demonstrating that by the 7th iteration, the path is already in the same region of the PES as the converged path. Included are the converged geometries for the minimum energy structures along the path.

04 June 2025 14:14:31

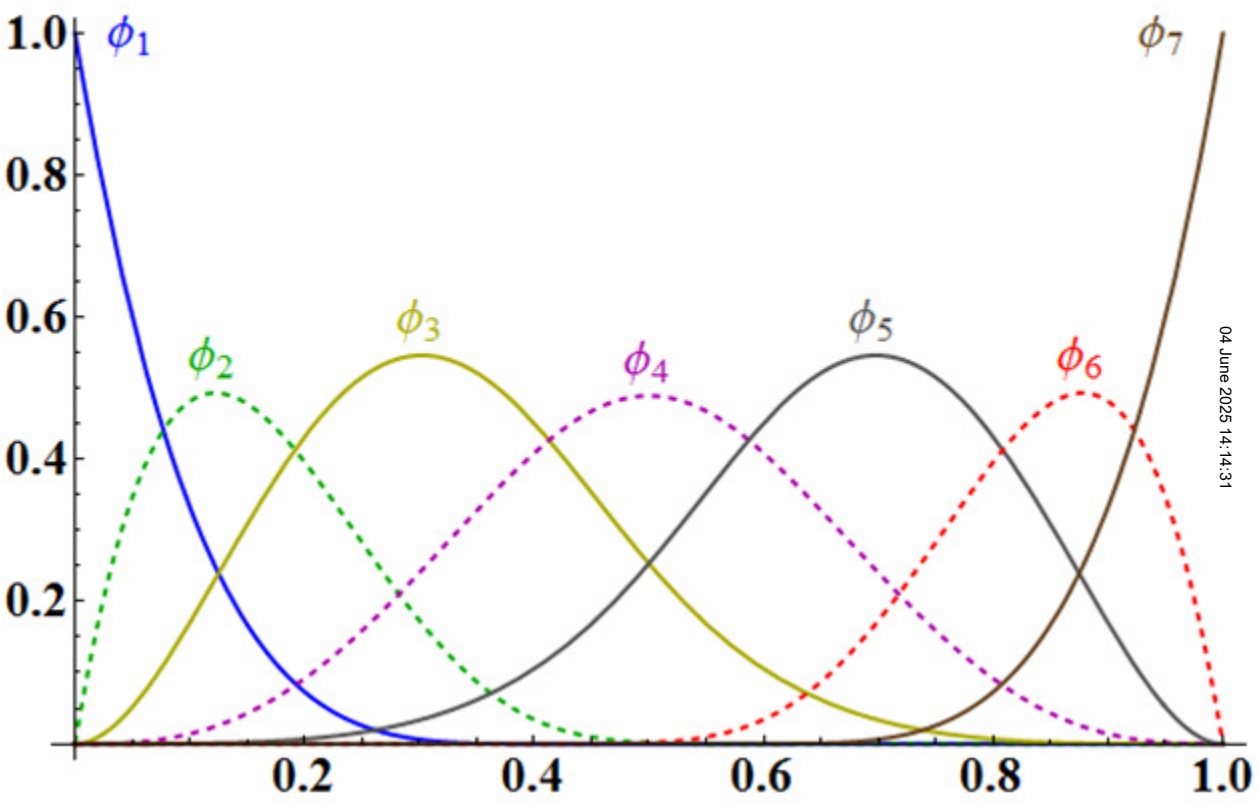
1.0
0.8
0.6
0.4
0.2
0.2
0.4
0.6
0.8
1.0
ϕ_1
ϕ_2
ϕ_3
ϕ_4
ϕ_5
ϕ_6
ϕ_7
04 June 2025 14:14:31

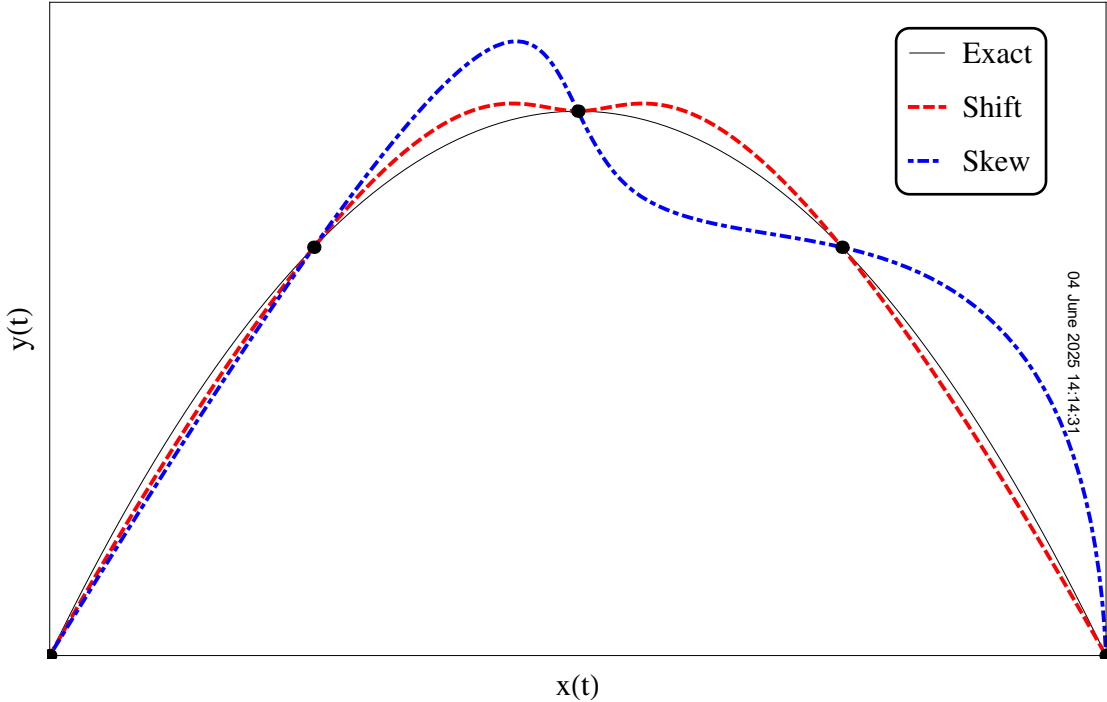
Exact
Shift
Skew
y(t)
x(t)
04 June 2025 14:14:31

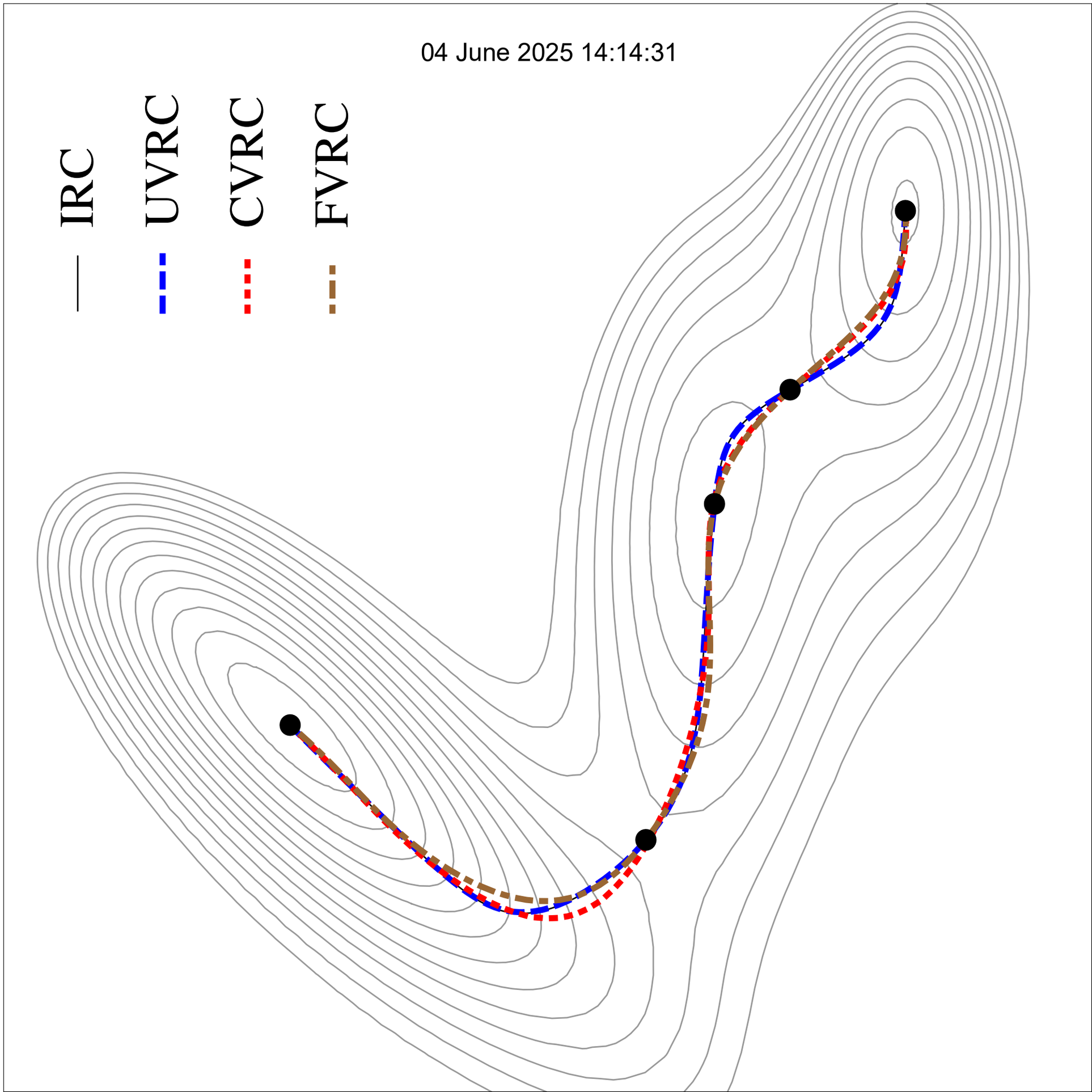
04 June 2025 14:14:31
IRC
UVRC
CVRC
FVRC

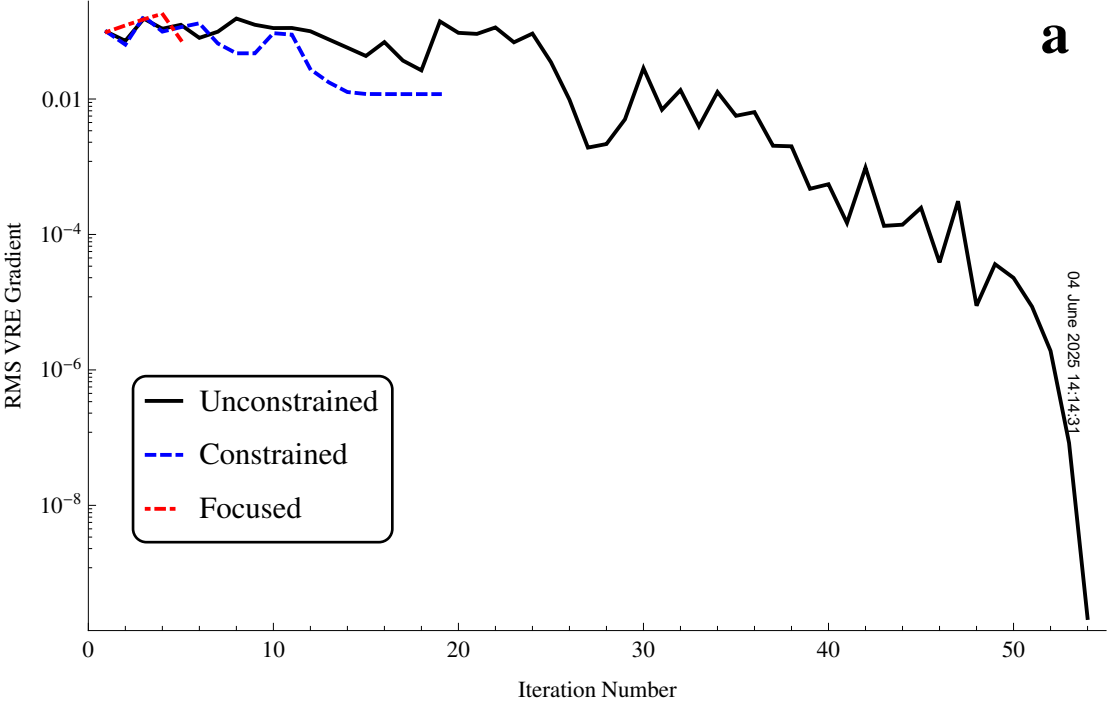
a
RMS VRE Gradient
0.01
10^{-4}
10^{-6}
10^{-8}
Unconstrained
Constrained
Focused
04 June 2025 14:14:31
0
10
20
30
40
50
Iteration Number

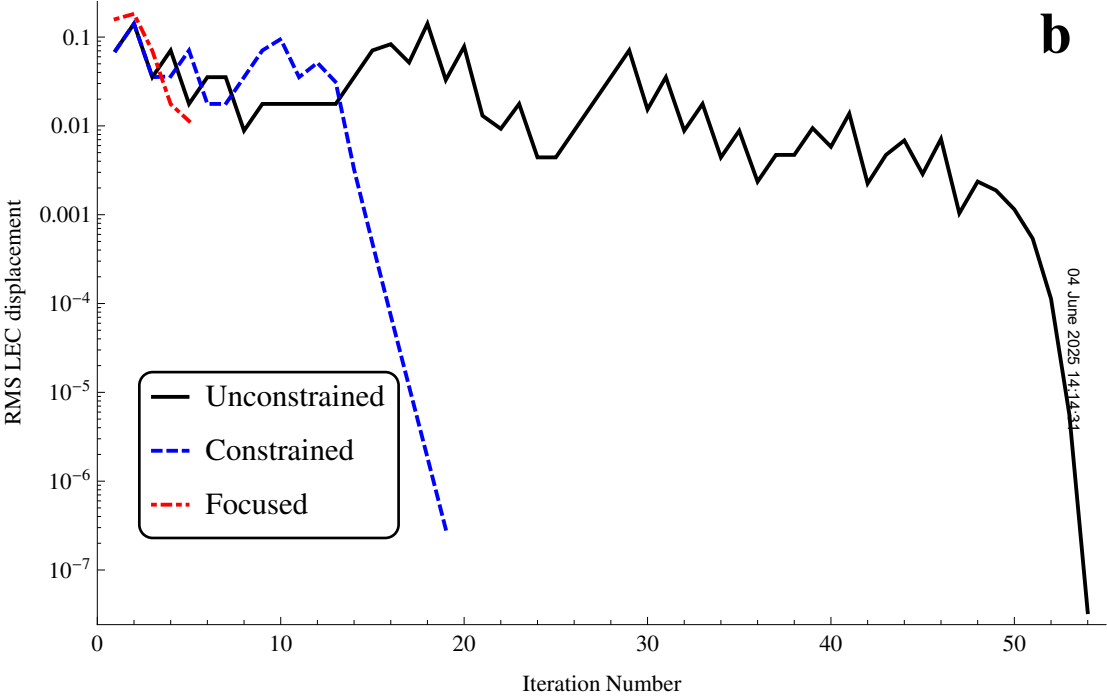
b
RMS LEC displacement
0.1
0.01
0.001
10^{-4}
10^{-5}
10^{-6}
10^{-7}
Unconstrained
Constrained
Focused
0
10
20
30
40
50
Iteration Number
04 June 2025 14:14:31

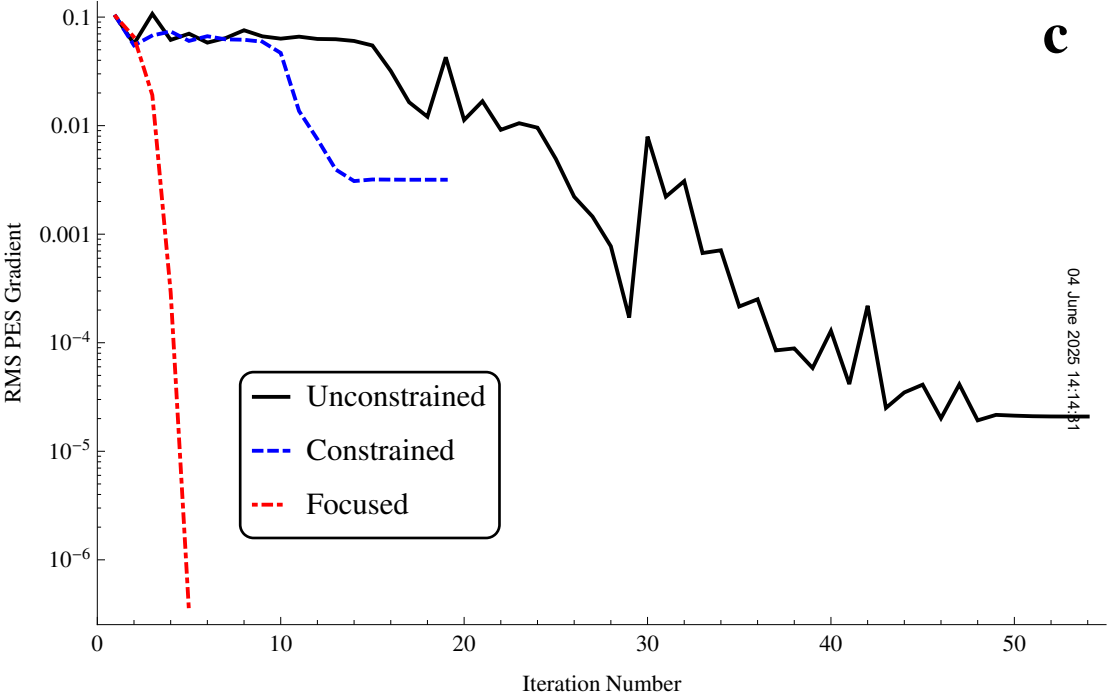
c
RMS PES Gradient
Iteration Number
Unconstrained
Constrained
Focused
0.1
0.01
0.001
10^-4
10^-5
10^-6
0
10
20
30
40
50
04 June 2025 14:14:31

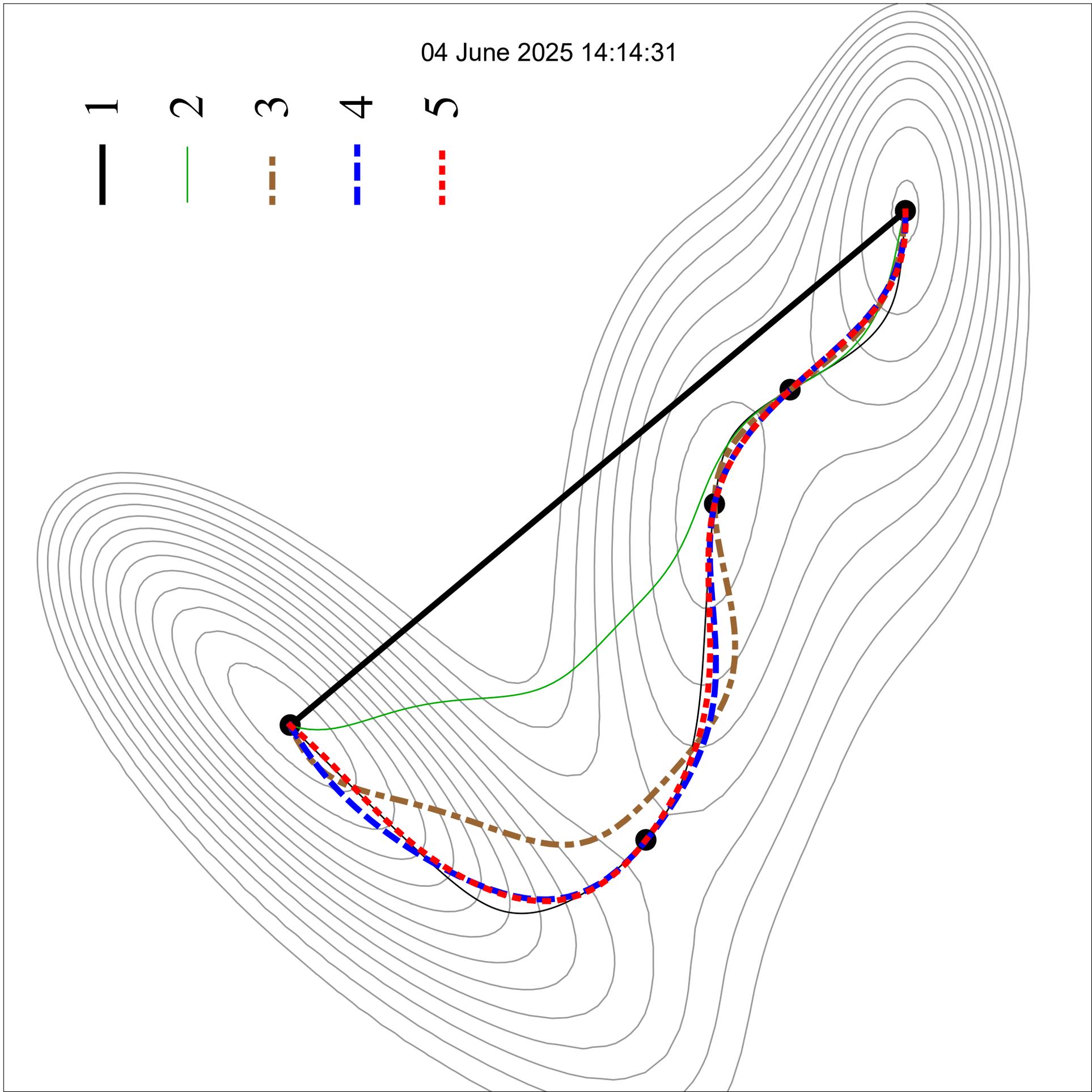
04 June 2025 14:14:31
1
2
3
4
5

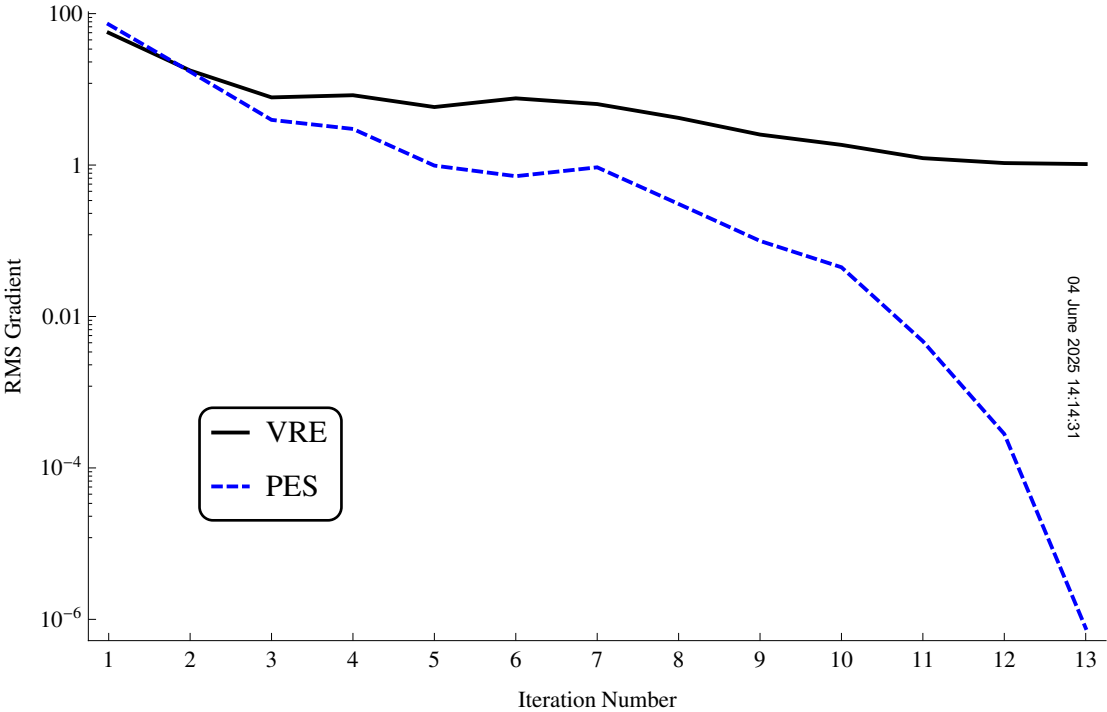
100
1
0.01
10^{-4}
10^{-6}
RMS Gradient
VRE
PES
04 June 2025 14:14:31
1
2
3
4
5
6
7
8
9
10
11
12
13
Iteration Number

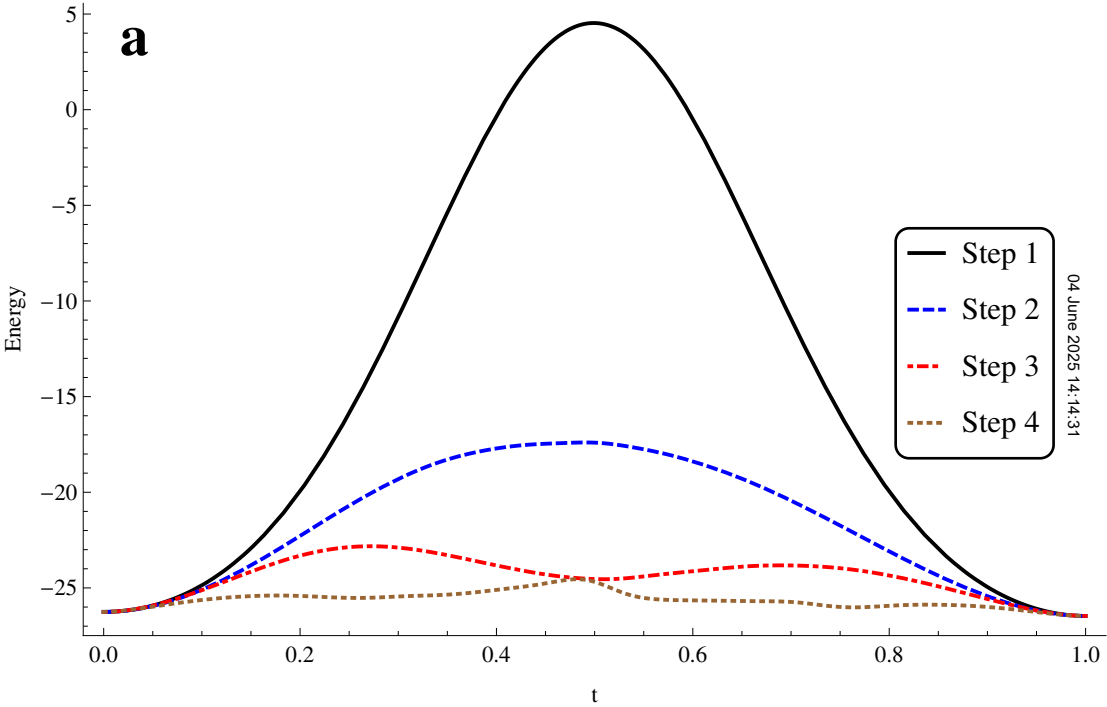
a
Energy
t
5
0
−5
−10
−15
−20
−25
0.0
0.2
0.4
0.6
0.8
1.0
Step 1
Step 2
Step 3
Step 4
04 June 2025 14:14:31

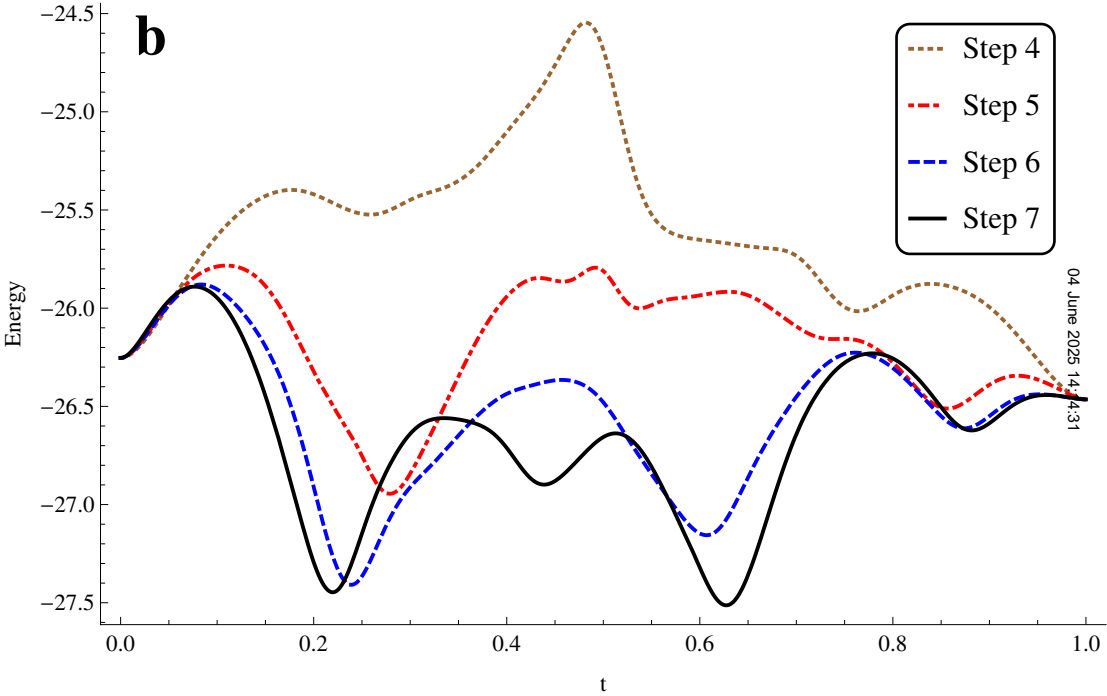
b
Step 4
Step 5
Step 6
Step 7
Energy
t
−24.5
−25.0
−25.5
−26.0
−26.5
−27.0
−27.5
0.0
0.2
0.4
0.6
0.8
1.0
04 June 2025 14:14:31

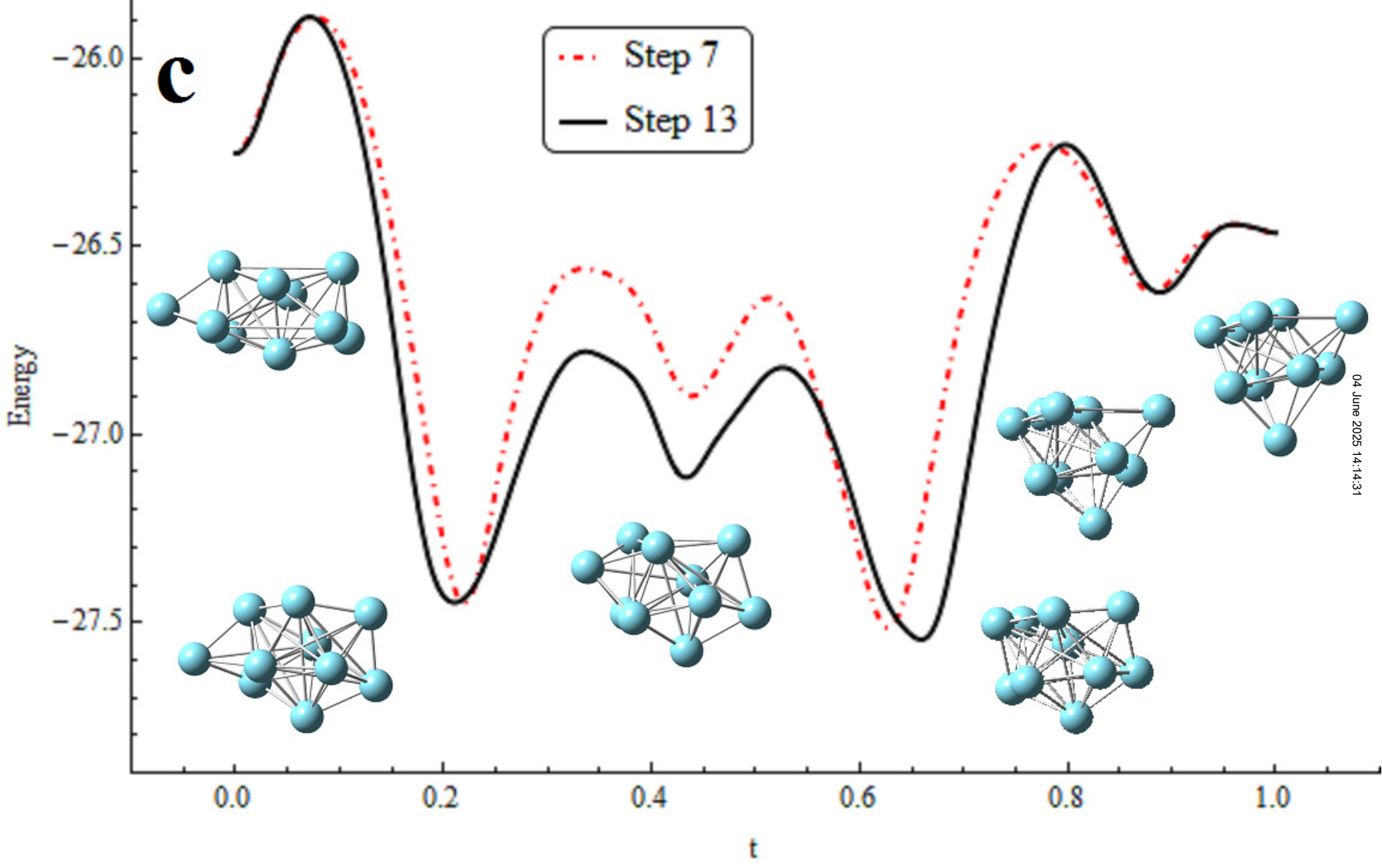

04 June 2025 14:14:31